Desalination and Water Treatment
www.deswater.com

doi: 10.5004/dwt.2022.28362

254 (2022) 116–141
April

Fe-encapsulated zeolite composite with free OH group as Fenton-like catalyst in near-neutral solution

Lei Wang[a], Chen Chen[a,*], Ting Cheng[b], Bo Ma[a], Run Zhou[a], Dianyi Wu[a], Xiao Zhang[b], Yuan Tian[a]

[a]*School of Environmental and Chemical Engineering, Jiangsu University of Science and Technology, Zhenjiang 212100, China, Tel. +86-0511-85639001; Fax: +86-0511-85639001; emails: chenc@just.edu.cn (C. Chen), yuwanlihuaxue@sina.com (L. Wang), 2424674288@qq.com (B. Ma), 2671621874@qq.com (R. Zhou), 836235866@qq.com (D. Wu), 1063894206@qq.com (Y. Tian)*
[b]*School of Environmental Ecology, Jiangsu City Vocational College, Nanjing 210017, China, emails: wnchengting@sina.com (T. Cheng), zhangxiao7376@sina.com (X. Zhang)*

Received 18 August 2021; Accepted 3 March 2022

ABSTRACT

A novel nano-scale zeolite encapsulated with iron ions (zeolite@Fe) was prepared, and used as a heterogeneous Fenton-like catalyst to participate in zeolite@Fe/H_2O_2 reaction. The zeolite@Fe material was characterized by X-ray diffraction, Fourier-transform infrared spectroscopy, scanning electron microscopy-energy-dispersive X-ray spectroscopy, and X-ray photoelectron spectroscopy, and the findings proved that zeolite@Fe was successfully achieved, and Fe^{3+} rich nano spherical-like shape material was formed on the surface of zeolite. The methylene blue (MB) was used to verify the catalytic activity of zeolite@Fe in Fenton-like reaction, and the reaction mechanisms were illustrated by spin-polarized density-functional theory computation. The experimental results stated that the addition of zeolite@Fe and H_2O_2 remarkable improved the degradation of MB. In addition, this Fenton-like reaction system could be achieved at a relatively wide and mild pH range. The temperature had a significant effect on zeolite@Fe/H_2O_2 reaction, and the reaction process could be better described by the first-order reaction kinetics model. Also, zeolite@Fe was stable in Fenton-like reaction after four times of reusing. Moreover, the findings of theoretical structure model and charge density distribution for zeolite@Fe suggested that •OH radicals forming by a large amount of free OH groups were the predominant reactive species responsible for MB degradation. Furthermore, after the complex interaction between H_2O_2 molecules and Fe elements, Fe active sites on the surface of zeolite@Fe were able to tear H_2O_2 molecules apart, forming a free OH group and H group while capturing one O element.

Keywords: Fenton-like reaction; Zeolite; Catalyst; Density-functional theory calculation; Theoretical structure model; Charge density distribution

1. Introduction

Recent years, a large amount of organic wastewater is continuously discharged to the receiving water in China. Organic wastewater, which is harmful to the human health and ecological environment, is mainly discharged from papermaking, leather, food production and other industries [1]. This type of wastewater often contains a great quantity of carbohydrates, fats, cellulose, and other organic substances [2]. If discharged directly, it could easily cause the water nutrition, the death of animals and plants, the destruction of soil structure, and other problems. Accordingly, appropriate treatment techniques for organic wastewater are continuously attracted more attention [3].

* Corresponding author.

At present, there exist many effective treatment methods for organic polluted wastewater, such as biological degradation [4–6], adsorption [7–9], classical oxidation techniques [10,11], etc. However, each treatment method has its own obvious advantages and disadvantages. The biological method has the advantages of high efficiency, low cost, convenient operation, and friendly environment, but the microorganism in biological degradation is difficult to domesticate. The adsorption is simple to be operated, whereas the recovery rate of adsorbent is relatively low, and in most situations the cost is relatively high. The reaction conditions of classical oxidation techniques are mild, and easy to control, whereas the strong oxidizers are expensive and the removal efficiencies are low.

The advanced oxidation process (AOPs) is a technique that directly mineralizes organic pollutants or increases the biodegradability of pollutants through the oxidation [12]. It exhibits great advantages in the treatment of environmental hormones and other trace harmful chemical substances. Meanwhile, AOPs can completely mineralize or decompose most organic substances. In this case, AOPs displays a better application prospect in the treatment of organic polluted wastewater [13–15]. Advanced oxidation technology commonly generates free radicals with strong oxidizing ability [12,14,16]. Under the reaction conditions of high temperature and high pressure, electricity, sound, light irradiation, or catalysts, the macromolecules in organic substances are oxidized into low-toxic or non-toxic small molecular substances. According to the different ways of free radicals generation and reaction conditions, advanced oxidation technology can be divided into photochemical oxidation [17,18], catalytic wet air oxidation [19], sonochemical oxidation [20], ozone oxidation [21], electrochemical oxidation [22], Fenton oxidation, and Fenton-like oxidation [23–25], and so forth.

Among them, the Fenton oxidation technique employs the chain reaction between Fe^{2+} and H_2O_2 to catalyze the generation of $^{\bullet}OH$ radicals, and the reagents consisting of Fe^{2+} and H_2O_2 are called Fenton reagents. According to literatures [14,26,27], Fenton oxidation technique displays extremely strong oxidizing properties, and it achieves the removal of pollutants through oxidizing various toxic and refractory organic compounds. In addition, this technique is especially suitable for the oxidation of organic wastewater [28,29]. In researches of Fenton oxidation reaction, it is reported that Fe^{2+} ions can be replaced by other substances, such as Fe^{3+} ions, iron-containing minerals [30,31], some transition metals (such as Cd, Co, Cu, Ag, and Mn) [32], composite catalyst including Fe(II)-activated CaO_2 [33], MgNCN/MgO nano-composites [34], 3D flower-like MgO_2 nanostructures [35], Graphitic N-rich graphene [36], and so forth. This type of reaction that accelerates or replaces Fe^{2+} and catalyzes H_2O_2 is called as a Fenton-like reaction [37,38].

In the conventional homogeneous Fenton-like oxidation technique, the catalyst is dissolved in the reaction system, so it is not easy to recycle after the reaction. Meanwhile, the amount of heavy metal sludge produced is relatively large and difficult to be disposed. In this case, there are many limiting factors in practical applications. In contrast, in the heterogeneous Fenton-like reaction technique, iron ions are fixed on a certain carrier. In this reaction, the adsorption material firstly adsorbs organic molecules to its surface, and degrades the organic molecules under the action of its stored iron ions and H_2O_2, and then the degradation products are returned to the solution after desorption [38]. This heterogeneous reaction technique can broaden the pH ranges of the reaction. Meanwhile, it avoids producing a large amount of heavy metal ions in solution and causing secondary pollution. At present, most of the research hotspots on heterogeneous Fenton-like reactions are focused on the choices of catalyst supports. Common carriers include composite metals, iron oxides, and organic materials, and so on [39–41].

The zeolite is a kind of aluminosilicate materials with an ordered microporous structure, which can effectively solve the problems of aggregation and stability. Zeolite is a general name of aluminosilicate materials, and this type of materials is orderly composed of silicon oxygen tetrahedron and aluminum oxygen tetrahedron. Because of its excellent stability, catalysis, and large specific surface area, zeolite was often used as catalyst carriers in chemical industrial processes [42–45]. Meanwhile, zeolite materials were often applied as the main carrier of Fenton-like reaction catalysts [46–49]. For example, Wang used bauxite and rice husk synthesized efficient heterogeneous Fenton-like catalysis of Fe-doped SAPO-44 zeolite [50]; Shi et al. [51] synthesized Fe doped PANI loaded on zeolite and applied as an active and recyclable Fenton-like catalyst; the zeolite Y promoted by Fenton's reagent ($FeSO_4$) and was applied for photo- Fenton-like oxidation of phenol by Guo et al. [52]; The recyclable Fenton-like catalyst based on zeolite Y supported Fe_2O_3 nanoparticles was synthesized by Yang et al. [53], and used for the removal of organics under mild conditions. At present, the main synthesis paths of zeolite Fenton-like catalysts concentrate on loading or encapsulating active heavy metal elements such as Fe into the surface or skeleton of zeolite materials. The main methods of loading and encapsulating heavy metals include ion exchange/adsorption [44,54], incipient wetness, incorporation of metal precursors [45,50,51], and mixed roasting [53].

In recent years, the zeolite Fenton-like catalysts with stable degradation effect and low cost have been attracted the attention of many researchers. In our previous research, a nano-scale zeolite material was synthesized and it displayed excellent adsorption capacity for heavy metals. In the following experiments, we used this material as the carrier [55,56]. Herein, this nano-scale zeolite material was utilized as a carrier to synthesize a Fenton-like catalyst. Through its excellent adsorption ability of Fe ions in the $Fe_2(SO_4)_3$ solution, a novel nano-scale zeolite encapsulated with iron ions (zeolite@Fe) was prepared and used as a heterogeneous Fenton-like reaction catalyst to participate in the reaction. Besides, the synthesis reaction was conducted at room temperature, the process was simple to operate, and the synthesized material was nano-scale in experiments. This research was to achieve the ideal degradation effect on organic matters, and provide an ideal technique or composite material for the Fenton-like reaction.

Moreover, the composite material was characterized by modern analytical instruments to identify its microscopic morphology, chemical composition and structure. The

methylene blue (MB) solution was used to verify the catalytic activity in zeolite@Fe/H_2O_2 system. The influence factors, including reaction temperature, reaction time, and pH values on the degradation efficiencies were investigated. Additionally, the stability and reusability of zeolite@Fe was evaluated through the reuse of Fenton-like reaction catalyst. Furthermore, the reaction mechanism in Fenton-like degradation reaction by zeolite@Fe catalyst was illustrated in this study. Besides, Vienna Ab initio Simulation Package (VASP) software and spin-polarized density-functional theory (DFT) computation were also used to conduct the theoretical structure model and its charge density distribution of zeolite@Fe. The experiments and theory calculation results proved that zeolite@Fe catalyst exhibited excellent activity and stability for the degradation of organic pollutant in solution.

2. Materials and experiments

2.1. Synthesis of catalyst

The synthesis method of nano-zeolite was consistent with our previous studies [55,56]. The synthesis steps of catalyst were as follows: Firstly, the nano-zeolite was synthesized, and the procedures were described as below, 6.1087 g of potassium silicate, 2.744 g of partial potassium aluminate, and 0.1819 g of directing agent ($[C_{18}H_{37}(CH_3)^2–N^+–(CH_2)^3–N^+–(CH_3)_2C_{18}H_{37}]Cl_2$) were weighed and added into a Teflon bottle containing 240 mL of potassium hydroxide solution, the concentration was 10 mol L^{-1}. A water bath reaction device was installed on a magnetic stirrer to keep the reaction temperature around 80°C. During the process of synthesis, the magnetic stirrer was maintained stirring and the reaction was performed for 10 h. After the synthesis reaction was finished, deionized water was used to wash the reaction products until the pH value of filter liquor was around 7. Then, the reaction product was dried at 105°C, and the obtained product was nano-zeolite (herein after referred to as zeolite). Secondly, 0.1 g of $Fe_2(SO_4)_3$ was added to 500 mL of deionized water, and stirred with magnetic stirrer until it was completely dissolved. Then, 0.1 g of above synthesized nano-zeolite material (zeolite) was added into the mixture to adsorb the Fe ions. After the adsorption was conducted for 30 min, the reaction solution was filter with 0.45 um membrane, and then the filter was washed with distilled water. After that, the solid product was dried in a blast drying oven until constant weight. Then, a novel nano-scale zeolite encapsulated with iron ions (zeolite@Fe) was obtained.

2.2. Characterization of catalyst

To illustrate the various properties of synthesized material, samples were fully characterized by liquid specific surface area, scanning electron microscopy-energy-dispersive X-ray spectroscopy (SEM-EDX), X-ray diffraction (XRD), X-ray photoelectron spectroscopy (XPS), and Fourier-transform infrared spectroscopy (FT-IR). The morphologies of material were examined with a HITACHI S-3400N scanning electron microscope. XRD patterns of powder samples were recorded by a Shimadzu XD-3A diffractometer, employing Cu-Kα radiation (λ = 1.54056 Å). The X-ray photoelectron spectroscopy spectra were examined by a PHI 5000 VersaProbe XPS equipment. The Fourier-transform infrared spectroscopy was recorded on a Bruker TENSIR 27 spectrophotometer with a resolution of 4 cm^{-1} using KBr disc. The liquid specific surface area is determined by Xigo liquid specific surface area measuring instrument. Moreover, the active species were detected by the Electron spin resonance, and using electron paramagnetic resonance spectrometer (EMXmicro-6/1/P/L, Karlsruhe, Germany). The DMPO (5,5-dimethyl-1-pyrroline N-oxide) was used as free radical ($^{\bullet}O_2^-$ and $^{\bullet}OH$) trapping agent to obtain the signals. Furthermore, to further investigate the reaction mechanism in the reaction process, the DFT calculation process was conducted through Vienna Ab initio Simulation Package (VASP) software [57] and spin-polarized DFT. The exchange-correlation potential was calculated by Perdew-Burke-Ernzerhof functional (PBE) [58,59] within the generalized gradient approximation (GGA) method [60,61]. In the process of calculation, the cut-off energy was 450 eV, and the K-points grids of dimensions were 5 × 5 × 5.

2.3. Degradation experiment

In each experiment, 0.1 g of zeolite@Fe catalyst and 4 mL of (30%) H_2O_2 solution (around 38.8 mM H_2O_2) was added into 100 mL of MB solution, the initial concentration was 20 mg L^{-1}, and stirred evenly with magnetic stirrer. The amount of oxidant added rate in this study was higher than that of other researchers [33,35,36], but it still belonged to the common concentration range of Fenton-like reaction in Table 3. Then, the mixtures were put into a transparent vessel on the magnetic stirrer at a specified temperature. After the reaction, a certain amount of liquid was drawn with an injection needle and filtered. The absorbance of wastewater after Fenton-like degradation was measured by ultraviolet visible spectrophotometer at 664 nm.

In the comparative experiments of reaction system, all experiments were carried out at 50°C and the reaction time was 40 min. The experimental condition of zeolite@Fe/H_2O_2 system was the same as above. In the Fe/H_2O_2 reaction system, 0.1 g of zeolite@Fe was replaced by 0.02 g of $Fe_2(SO_4)_3$, and the content of Fe was basically the same as that of 0.1 g of zeolite@Fe. In zeolite@Fe reaction system, there was no H_2O_2 added. In H_2O_2 reaction system, there was no addition of zeolite@Fe. In zeolite reaction system, 0.1 g of zeolite@Fe was replaced by 0.1 g of original zeolite. During the effect of comparative experiments, all tests were also carried out at 50°C and the reaction time was 40 min. The initial pH value was ranged from 5 to 8. The concentration of CO_3^{2-}, HCO_3^-, F^-, Cl^-, and PO_4^{3-} was all 2 mmol L^{-1} and prepared from Na_2CO_3, $NaHCO_3$, NaF, NaCl, and Na_3PO_4, respectively. When investigating the influence of reaction temperature and time, the reaction time was ranged from 0 to 100 min, and the reaction temperature was ranged from 30°C to 60°C.

To estimate the stability and reusability of catalytic performance of zeolite@Fe in Fenton-like reaction, the consecutive cycles were done to measure the catalytic degradation efficiencies of MB. At the same time, the morphology and patterns of recycled catalytic material were evaluated. After each recycled experiment, the catalyst was filtered out from the solution by 0.45 μm filter membrane, and the filer solids were washed by deionized water for several times.

Then, the product was dried to constant weight at a temperature of 85°C in the blast drying oven for the next cycle. The Fe element dissolved in the reaction system was measured with an AA240DUO atomic absorption spectrometer. All the recycle experiments were carried out at 50°C and the reaction time was 40 min.

Furthermore, to illustrate the possible mechanism of catalytic reaction in Fenton-like system, the active species generated in the process of catalytic degradation reaction were analyzed, and different trapping agents were put into the reaction mixtures. These scavengers included 0.01 mL of TBA (*tert*-butyl alcohol), 0.0108 g of BQ (1,4-benzoquinone), 0.1 g of EtOH (ethanol), 0.2 g of IPA (isopropanol), and 0.01 g of FFA (furfuryl alcohol).

3. Results and discussions

3.1. Liquid specific surface area

The specific surface area was one of the important properties of catalysts. Catalysts with higher specific surface area could provide sufficient reaction interface and contribute to the improvement of catalytic efficiency. In this research, the liquid specific surface area results of zeolite and zeolite@Fe were deducted based on the fitting results of computer, as shown in Fig. 1. According to the fitting results, the liquid specific surface area of zeolite and zeolite@Fe were 1,211 and 1,326 m^2 g^{-1}, respectively, which was similar to those of previous studies [55]. Also, the liquid specific surface area of zeolite@Fe was larger than that of zeolite, and that demonstrated the liquid specific surface area of composite material might be increased through the adsorption of Fe.

3.2. X-ray diffraction

The XRD technology could effectively analyze the mineral phase composition of materials. XRD patterns of original zeolite and zeolite@Fe are depicted in Fig. 2a. The main peaks of original zeolite could be found at 2θ: 12.6° (1 1 0), 13.6° (0 0 2), 18.5° (1 1 2), 21.1° (2 1 1), 25.5° (2 2 0), 27.1° (0 0 4), 28.5° (3 1 0), 28.9° (1 0 0), 29.98° (1 1 4), 31.6° (3 1 2), 39.8° (3 1 4), 43.2° (4 1 3), and 52.4° (4 4 0) [55]. These curves were corresponded to the standard peaks of PDF#38-0216 ($KAlSiO_4$). Although all the zeolites were constructed with silica tetrahedron and alumina tetrahedron as basic units, each zeolite had different crystal structure. As a common carrier of Fenton-like reaction, clinoptilolite was the main component of natural zeolite [62–64]. Both its crystal structure and chemical composition were different from those of the minerals studied in this research, which would lead to different adsorption and binding action of Fe ions.

The main peaks of zeolite@Fe material could also be found at 2θ: 12.8°, 13.6°, 18.7°, 21.4°, 25.1°, 27.3°, 28.7°, 29.1°, 30.3°, 31.8°, 39.6°, 43.2°, and 52.5°, indicating the adsorption of Fe did not change the crystal structure of the material, and that also suggested zeolite@Fe catalytic material was successfully fabricated. In addition, some peaks of zeolite@Fe including 2θ at about 12.8°, 28.7°, 29.1°, 30.3°, 31.8° and 39.6° were obviously lower than that of the original zeolite. It was believed that the intensity of the crystal diffraction peak was directly related to the crystallinity of the crystal, and the peak height and intensity of XRD diffraction peaks of crystals with higher crystallinity were generally higher. Researchers had used the intensity values of the crystal diffraction peaks to compare the relative crystallinity of various materials [65,66]. These findings implied that the adsorption of Fe contributed to the decrease of crystal integrity, which was similar to the results of other researches [67,68].

3.3. Fourier-transform infrared spectroscopy

FT-IR analysis could better obtain the information of the functional group structure of materials. The FT-IR results of zeolite@Fe catalyst are described in Fig. 2b, and the

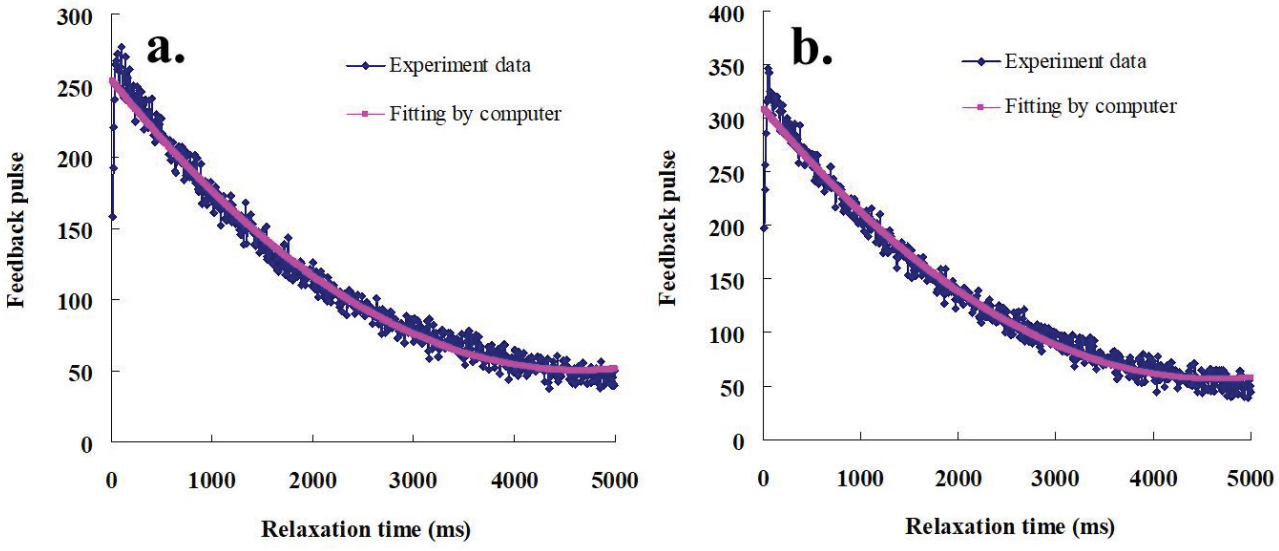

Fig. 1. Liquid specific surface area of zeolite and zeolite@Fe.

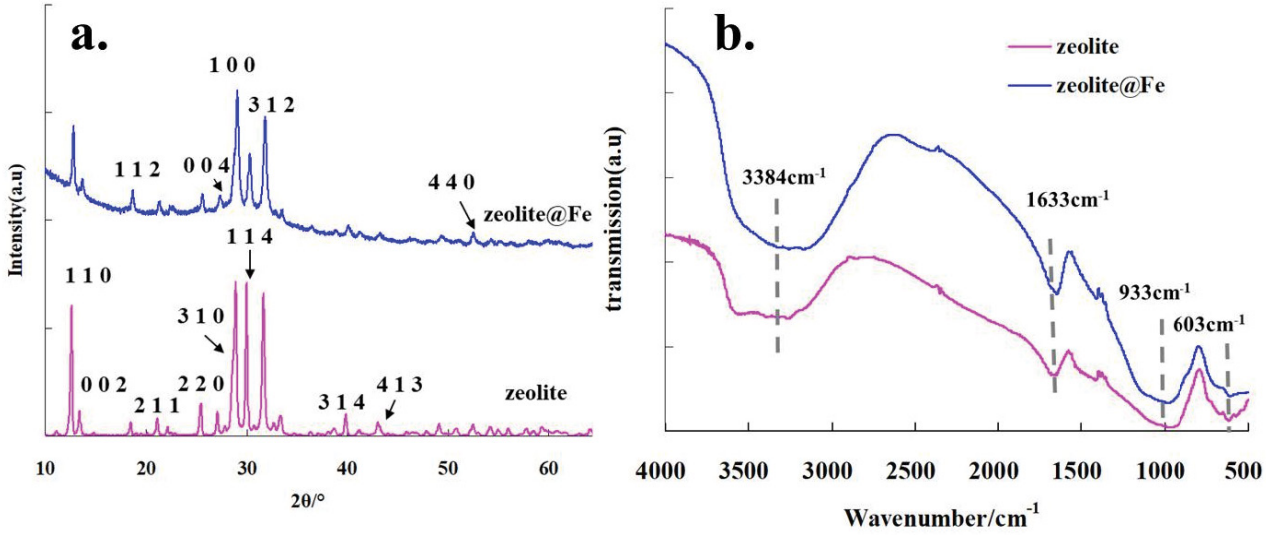

Fig. 2. XRD analysis of original zeolite and zeolite@Fe catalyst (a) and FT-IR analysis of original zeolite and zeolite@Fe catalyst (b).

original nano-zeolite was also measured as a comparison. The main infrared curves of both materials were appeared at 3,384; 1,633; 933 and 603 cm^{-1}. The peaks of 3,384 and 1,633 cm^{-1} were matched with the stretching vibration of the O–H group, which came from the adsorbed water in material [69]. In addition, the infrared peak at 603 cm^{-1} was attributed to the bending vibration of the O–Si(Al)–O group [56,69]; and the infrared peak at 933 cm^{-1} was ascribed to the stretching vibration of Si(Al)–O–Si(Al) [56,69]. Combined with our previous research findings [56,70], the main group in both materials were composed of Si(Al)–O tetrahedron structure, which was the basic structure of a typical zeolite material. This analytical result demonstrated that there was almost no change in the chemical bonds and basic structure between original zeolite and zeolite@Fe catalyst.

3.4. Scanning electron microscopy-energy-dispersive X-ray spectroscopy

The microscopic morphology and elemental composition of materials directly affected the macroscopic properties. To further observe the microscopic morphology and composition of zeolite@Fe and original nano-zeolite, the SEM and EDX analysis of samples were applied, and the results are depicted in Figs. 3 and 4. In previous researches, by adding a template named $[C_{18}H_{37}(CH_3)^2–N^+–(CH_2)_3–N^+–(CH_3)_2C_{18}H_{37}]Cl_2$ in the synthesis process of zeolite, nano-zeolite could be successfully synthesized [56,71]. It could be seen from Fig. 3 that the synthesized zeolite (original zeolite, white powder) was belonged to tetragonal crystal type, and the size was ranged from 200 to 500 nm. Also, the zeolite had a smooth surface. From the EDX analysis, it could be known that the main chemical composition (atomic percentage/%) of original zeolite was Al (14.5%), Si (14.02%), K (13.03%), and O (58.45%), which was close to the chemical formula of zeolite PDF#38-0216 ($KAlSiO_4$).

Moreover, it was observed from Fig. 4a and b that the nano-range tetragonal crystal also could be found, but the surface became very rough. After the adsorption process, the Fe^{3+} was distributed on the surface of the zeolite in a nano spherical-like shape, and the sphere size was between 100 and 400 nm. In addition, the color of zeolite@Fe changed to dark yellow. In order to clarify its composition, the sample was also analyzed by EDX, as shown as Fig. 4c and d. The results of EDX analysis indicated that compared with the constituent elements of pure nano-zeolite, composing of Si, Al, and K, only the element of Fe was added to the constituent elements of amorphous substance wrapped the surface.

The main chemical content (atomic percentage/%) of each element was as follows: Al (14.36%), Si (15.08%), K (6.17%), Fe (2.1%), and O (62.3%). Changes of Fe and K content implied that Fe^{3+} replaced three K^+ in zeolite crystals during the adsorption process. Furthermore, more details could be found from the EDX line (Fig. 5a and b) and element mapping analysis (Fig. 5c–g) results of zeolite@Fe crystals. From Fig. 5a and b, it could be seen that all the elements including Al, Si, O, K, and Fe were distributed on the energy spectrum analysis line (about 6 μm). The CPS strengths of O, Al and Si were much stronger than that of K and Fe. Similar results could be obtained from the element mapping analysis. From Fig. 5c–g, it could be known that all the nano spherical-like shape materials (Fig. 5a) contained elements of Al, Si, O, K, and Fe. Besides, the element distribution intensity of K and Fe was much lower than that of Al, Si, and O. The total chemical content (atomic percentage/%) of elements in analysis line was as follows: Al (14.4%), Si (14.3%), K (2.2%), Fe (4.6%), and O (61.5%). The increase of Fe content indicated that Fe element was more concentrated in the nano spherical-like shape materials. Considering that there was no obvious new crystal phase in XRD results of zeolite@Fe (Fig. 2a) and zeolite had strong ion exchange capacity, nano spherical-like shape materials might be the reaction product of ion exchange between Fe^{3+} ions in solution and K^+ ions in zeolite. In a word,

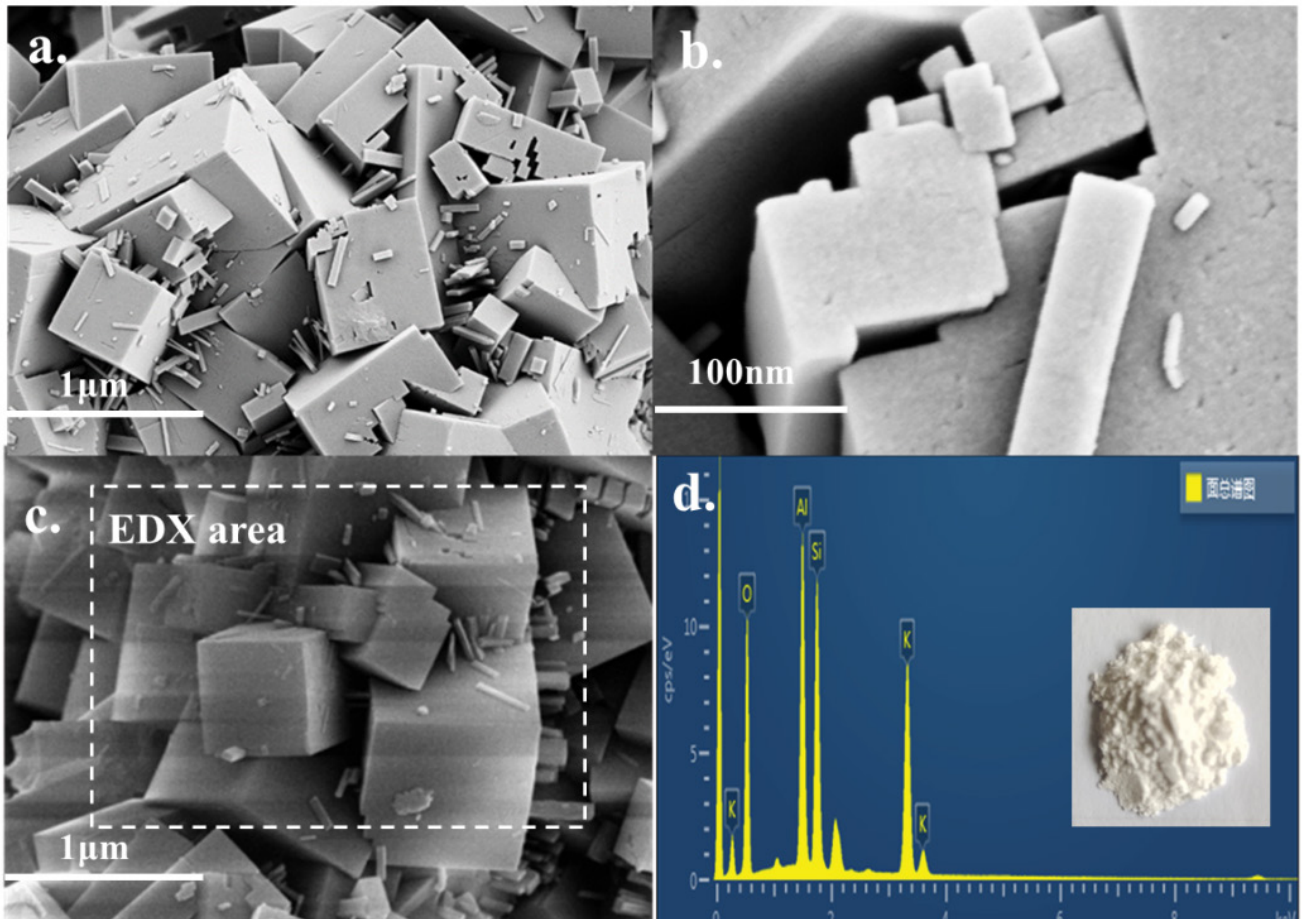

Fig. 3. SEM and EDX analysis of original zeolite.

after the adsorption of Fe^{3+}, some Fe rich nano spherical-like shape materials successfully formed on the surface of zeolite.

3.5. X-ray photoelectron spectroscopy

The chemical composition and surface electronic states could be gained from XPS technology. In experiments, the original zeolite and zeolite@Fe were examined by the XPS spectroscopy, as shown as Figs. 6 and 7. It was observed that the mainly peaks of pure original zeolite were Al2p (73.76 eV), Si2p (101.56 eV), C1s (293.25 eV), K2p (293.3 eV), and O1s (530.82 eV). Except for C1s (test needs), the other elements were consistent with previous experimental results [56]. The chemical composition (atomic percentage/%) of original zeolite gained from XPS analysis was Al (15.1%), Si (15.3%), K (12.9%), and O (56.9%), which was similar with the molecular formula as $KAlSiO_4$. The strong Si2p (Fig. 6b) and Al2p (Fig. 6c) peaks in the high-resolution XPS spectra results further verified the existence of zeolite structure. The K2p peaks split into two peaks. According to the peak position and intensity ratio, the two peaks should be belonged to $K2p_{1/2}$ and $K2p_{3/2}$, which confirmed the existence of K^+ in the original zeolite. The strong peak of O1s could also be divided into two peaks at 531.6 and 530.8 eV, owning to the difference between Si–O bond and Al–O bond in tetrahedral unit structure.

Fig. 7 shows the XPS analysis results of zeolite@Fe. It is observed that the main peaks of zeolite@Fe are Fe2s (839.1 eV), Fe2p (711 eV), O1s (531.36 eV), K2s (379.08 eV), K2p (293.03 eV), C1s (284.64 eV), Si2p (100.21 eV), and Al2p (74.21 eV). All the other constituent elements could be found in original zeolite except for Fe2s and Fe2p. The chemical composition gained from XPS was as follows: Al (14.6%), Si (14.9%), K (6.3%), Fe (2.8%) and O (61.4%), and that almost corresponded to the results of EDX. Also, the high-resolution XPS spectra of K2p were similar to the previous results of original zeolite. Besides, the decreasing of peak intensity suggested that K atom was partly replaced by Fe atom during the adsorption process. The high-resolution XPS spectra of Al2p and Si2p for zeolite@Fe catalyst were shown in Fig. 7b and c, respectively. After the peak fitting, both the Al2p and Si2p spectra could be decomposed into two individual peaks (100.8 and 101.9 eV) and (74.1 and 74.8 eV). The appearance of new peaks (74.8 and 100.8 eV) might indicate that the Si–O bond and Al–O bond in the tetrahedral structure had been partly changed because of the adsorption of Fe^{3+}. Simultaneously, the O1s peaks (Fig. 7e) could be divided into three peaks including 530.8, 531.5, and 533.3 eV. The peaks at 530.8 and

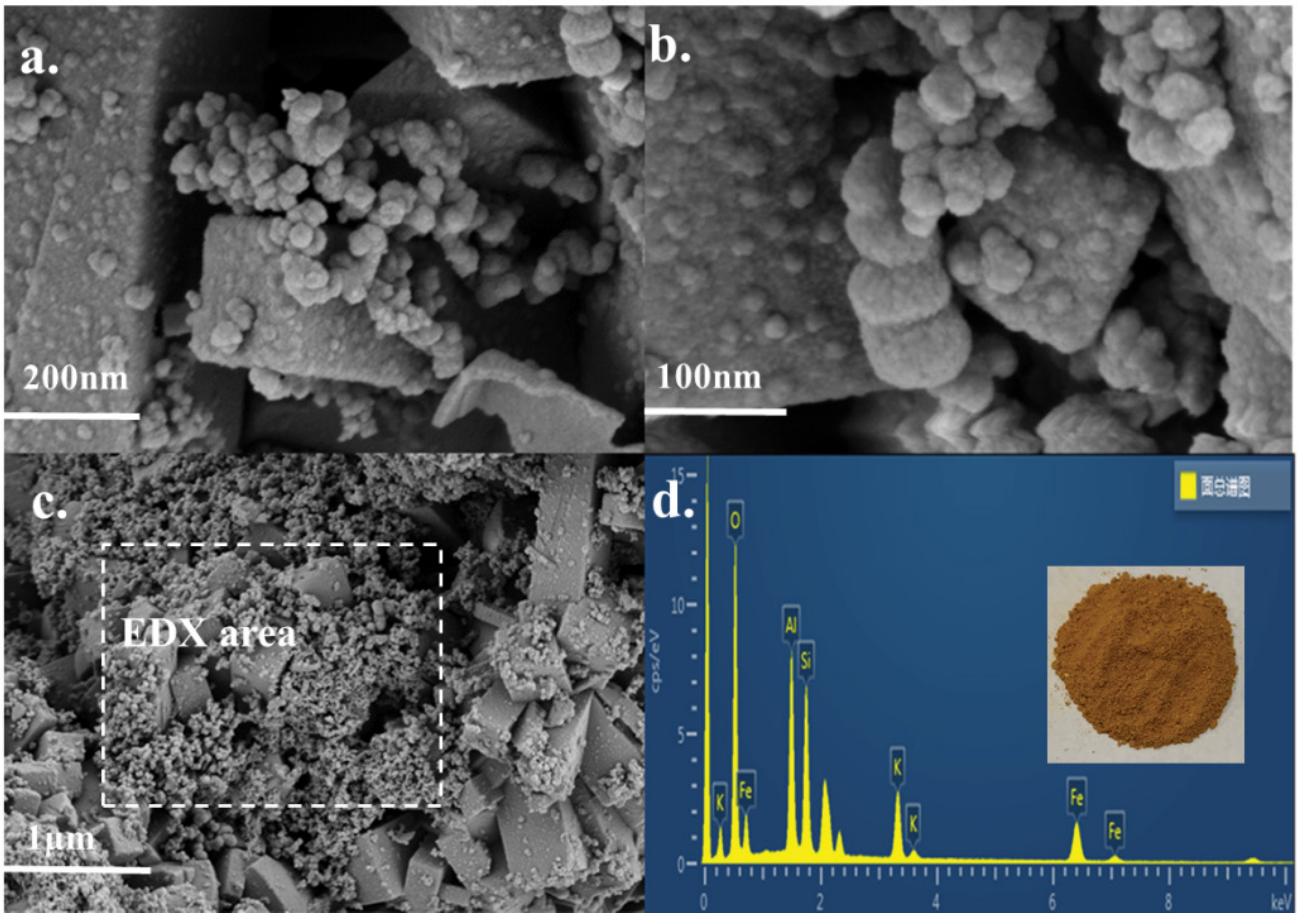

Fig. 4. SEM and EDX analysis of zeolite@Fe.

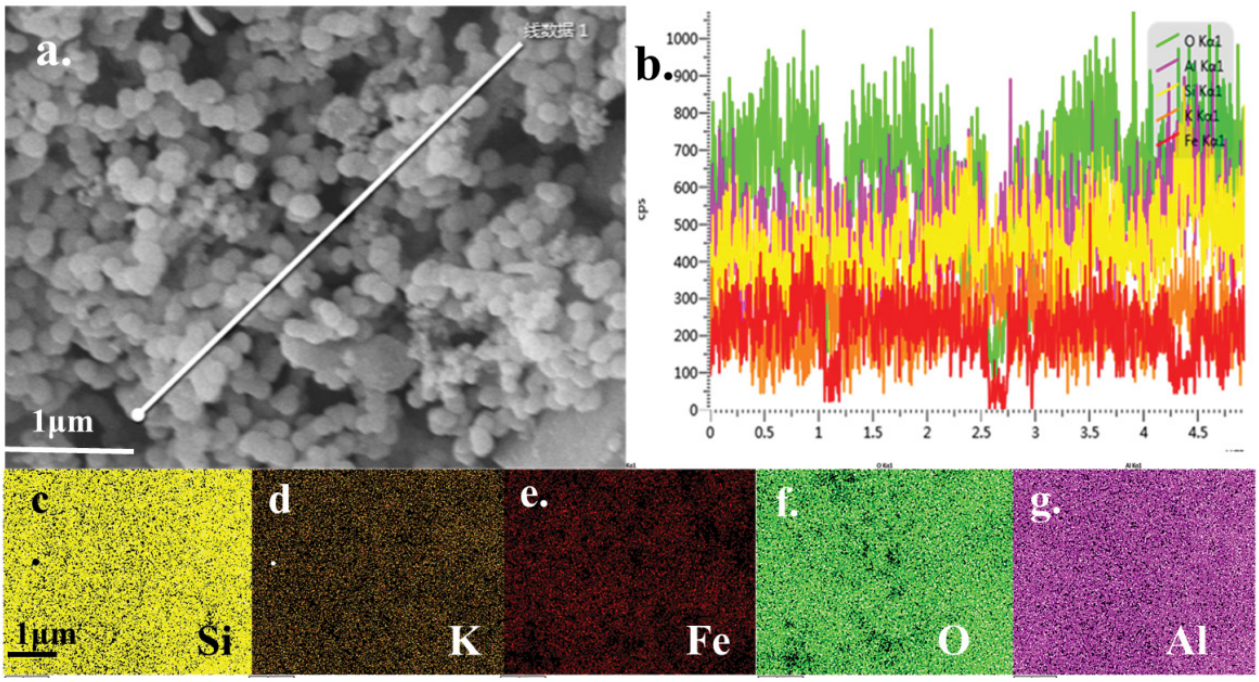

Fig. 5. The EDX line and element mapping analysis results of zeolite@Fe.

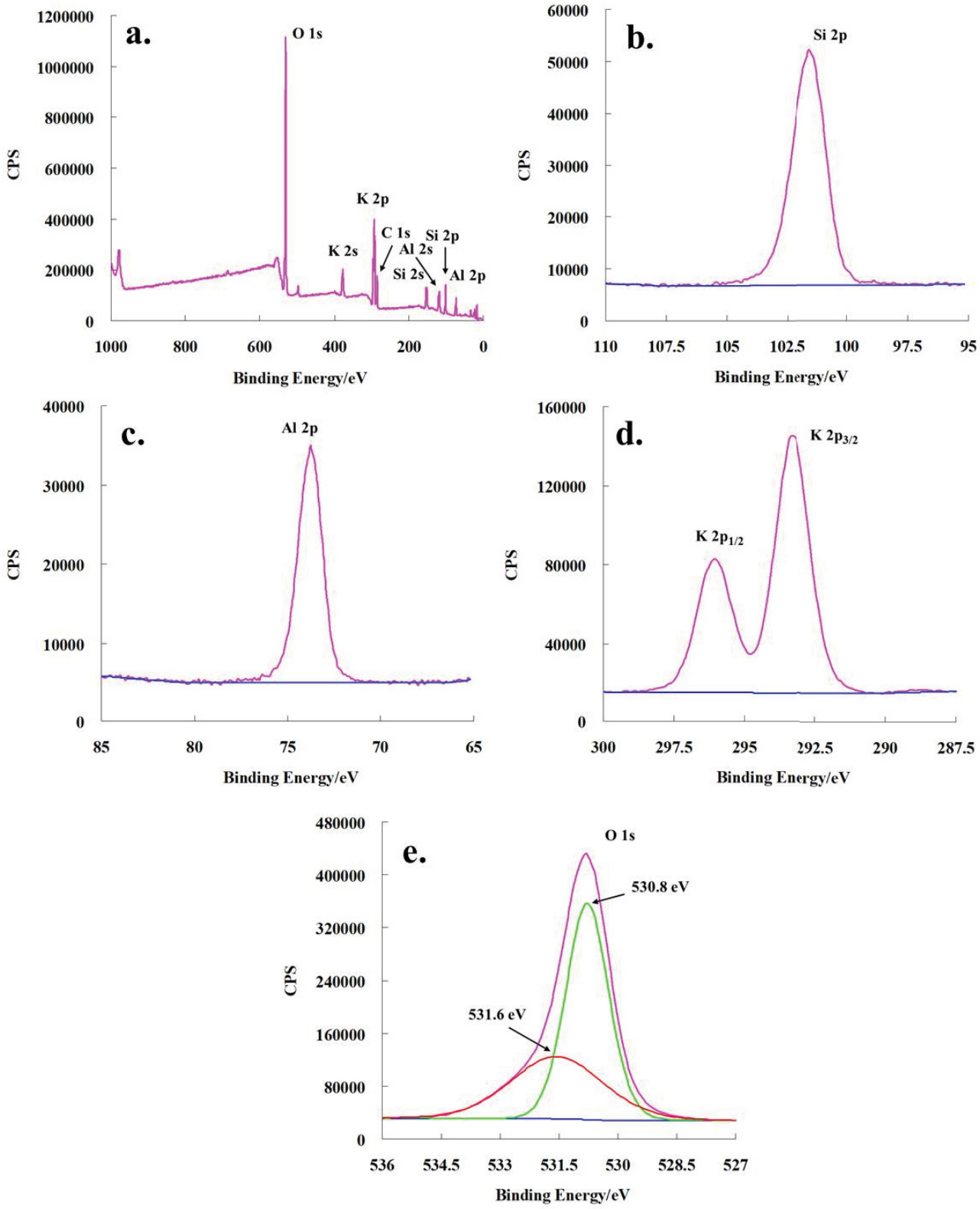

Fig. 6. Full XPS spectrum scanning analysis of original zeolite (a) and the high-resolution XPS spectra of Si2p (b), Al2p (c), K2p (d) and O1s (e).

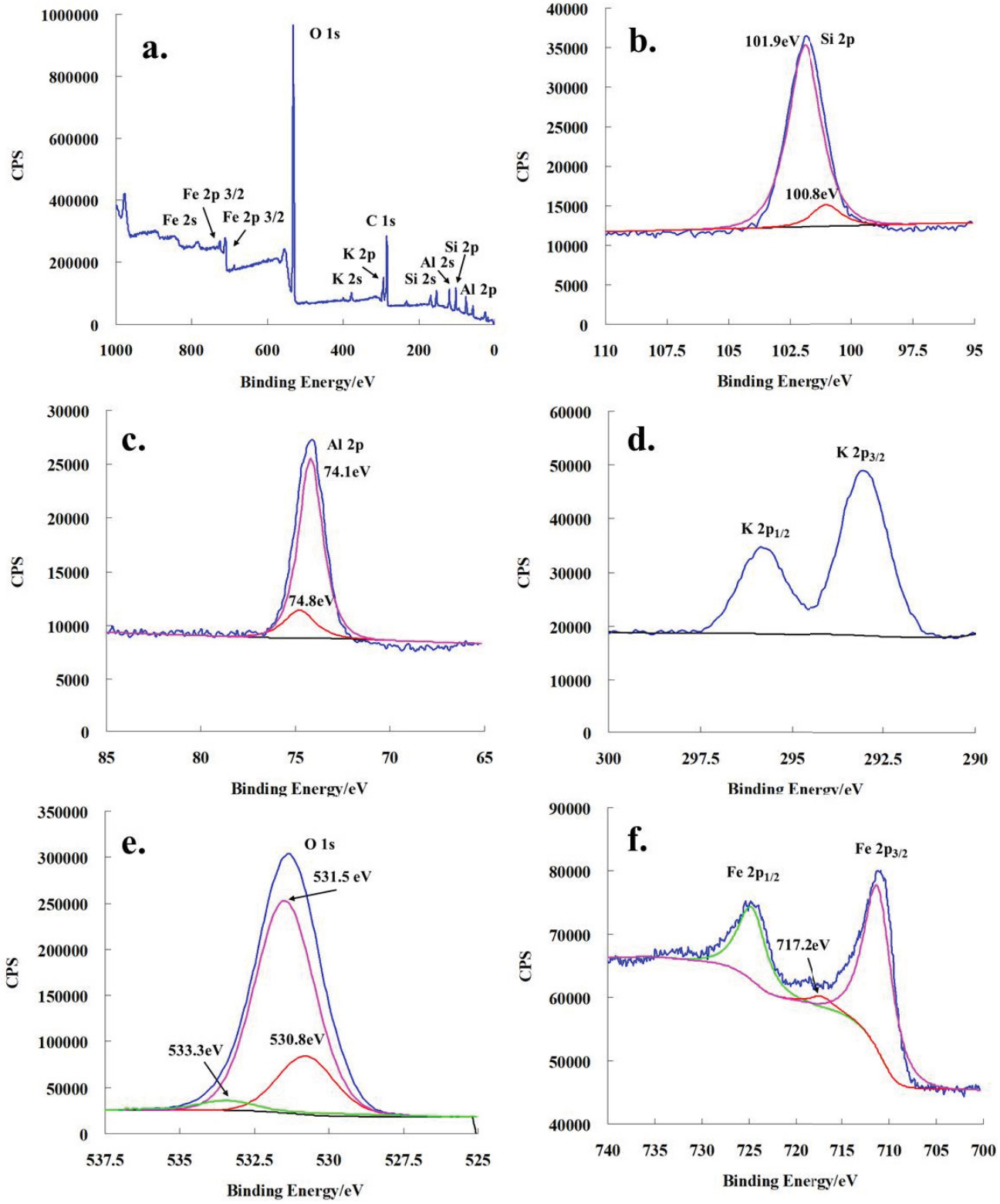

Fig. 7. Full XPS spectrum scanning analysis of zeolite@Fe (a) and the high-resolution XPS spectra of Si2p (b), Al2p (c), K2p (d), O1s (e) and Fe2p (f).

531.5 eV also could be found in the O1s peaks of original zeolite. The new small peak at 533.3 eV also could be explained as the partly changed transformation of Si–O bond and Al–O bond in the tetrahedral structure. Furthermore, the high-resolution XPS spectrum of Fe2p was shown in Fig. 7f. As Fig. 7f shown, two strong peaks around binding energies of 725.71 and 712.21 eV could be found. According to the peak position and relative strength, the two peaks could be attributed to $Fe2p_{1/2}$ and $Fe2p_{2/3}$. Meanwhile, a shoulder peak at 717.2 eV was corresponded to the satellite peak. Based on related references, the binding energies of Fe2p were similar to those of Fe^{3+} in α-Fe_2O_3 [31,72]. These findings indicated the iron element in zeolite@Fe was trivalent iron. Finally, the above XPS analysis proved the element composition and state of original zeolite and zeolite@Fe.

3.6. Catalytic activity of zeolite@Fe in Fenton-like system

In experiments, MB was chosen as a target pollutant to evaluate the catalytic activity of zeolite@Fe in Fenton-like reaction. Meanwhile, a series of control experiments were conducted to compare the degradation efficiencies of pollutant under different conditions, as shown as Fig. 8. It was seen that after 40 min reaction, the removal of MB was negligible in the solutions containing H_2O_2 alone, suggesting MB was stable in the presence of H_2O_2 [73]. The adsorption efficiency of MB onto zeolite reached 35.6% in the first 10 min, but the absorption efficiency was hardly decreased afterwards. This could be explained that the pure nano-zeolite displayed some adsorption effect on MB. While when the adsorption equilibrium was reached, the amount of MB in the wastewater was stable. Compared to the degradation efficiency of pure nano-zeolite, the adsorption efficiency of zeolite@Fe was slightly worse, only about 7% of MB was removed after adsorbing for 20 min, and the adsorption reached equilibrium in 40 min. This might

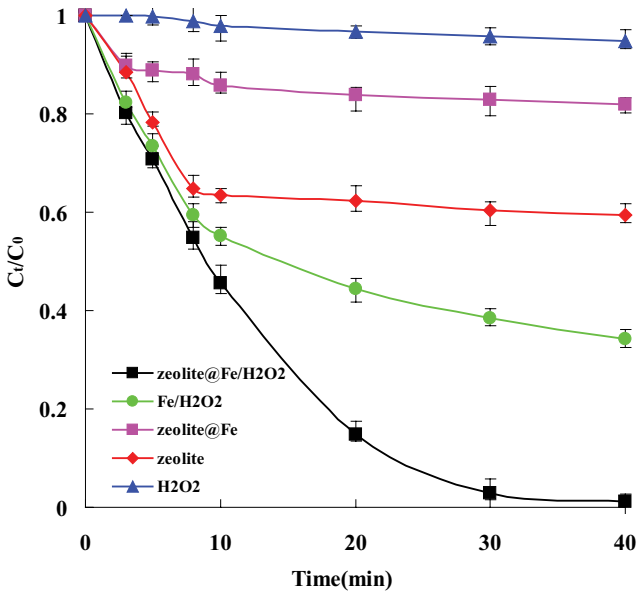

Fig. 8. Degradation of MB under different reaction systems.

due to a considerable part of the adsorption sites on zeolite were occupied by Fe^{3+} ions. For the traditional homogeneous Fenton degradation system (Fe/H_2O_2), the removal rate of MB reached 66% after 40 min. While zeolite@Fe and H_2O_2 were added into MB solution, a remarkable MB degradation was obtained. After 40 min of reaction, the degradation efficiency of MB was achieved 99.2%. Meanwhile, the treatment effect of zeolite@Fe was obviously better than that of classic homogeneous Fenton degradation system (Fe/H_2O_2) and other systems. Hence, it was concluded that the addition of zeolite@Fe material obviously accelerated the catalytic activity in Fenton-like reaction.

3.7. Effect of solution composition

It is generally believed that the solution composition (including solution pH and coexisting anions) of the reaction system would have a great impact on the degradation effect of pollutants. First of all, the pH value is an important factor that significantly affects Fenton and Fenton-like oxidation of organic compounds [51,74,75]. Generally speaking, the optimal pH for the conventional homogeneous Fenton reaction is harsh and in acidic condition. However, considering the industrial process, the pH value of the reaction system should be kept as mild as possible to avoid strong acid and alkali system. Hence, the selected pH range in this experiment ranged from 5 to 8, as shown as Fig. 9a. It could be seen from Fig. 9a that the degradation efficiencies of MB did not change much with the increase of initial pH value. Also, in the degradation systems at different pH values, the target pollutant could be almost completely removed within 40 min, indicating the requirements for pH values in this zeolite@Fe/H_2O_2 system were not as harsh as the traditional homogeneous Fenton reaction, and the Fenton-like reaction could be carried out in relatively wide and neutral reaction environment.

Fig. 9b shows the effect of coexisting anions (including CO_3^{2-}, HCO_3^-, F^-, Cl^-, and PO_4^{3-}) on the degradation of MB in zeolite@Fe/H_2O_2 system. It could be presented that the existence of F^- or PO_4^{3-} had the greatest impact on the degradation of pollutants, mainly because both the F^- and PO_4^{3-} were considered to have the capturing abilities for many reactive radicals [76]. Meanwhile, CO_3^{2-} also had a great influence on the degradation efficiencies, mainly because CO_3^{2-} could capture $^{\bullet}OH$ in the system and the presence of CO_3^{2-} would lead to the increase of solution pH in reaction system [77]. Finally, the existence of Cl^- and HCO_3^- had the negative effect on the reaction process, mainly because Cl^- and HCO_3^- could react with $^{\bullet}OH$ to form less active chlorine/hypochlorous/carbonate radicals.

3.8. Effect of reaction temperature and time

Fig. 10 presents the effect of reaction temperature and reaction time on MB degradation in zeolite@Fe/H_2O_2 system. It was obvious that with the rises of reaction temperature, the removal rates of pollutant were greatly increased. In experiments, we observed that the removal efficiencies of MB were not ideal and it took a relatively long time to degrade pollutant when the reaction temperature was

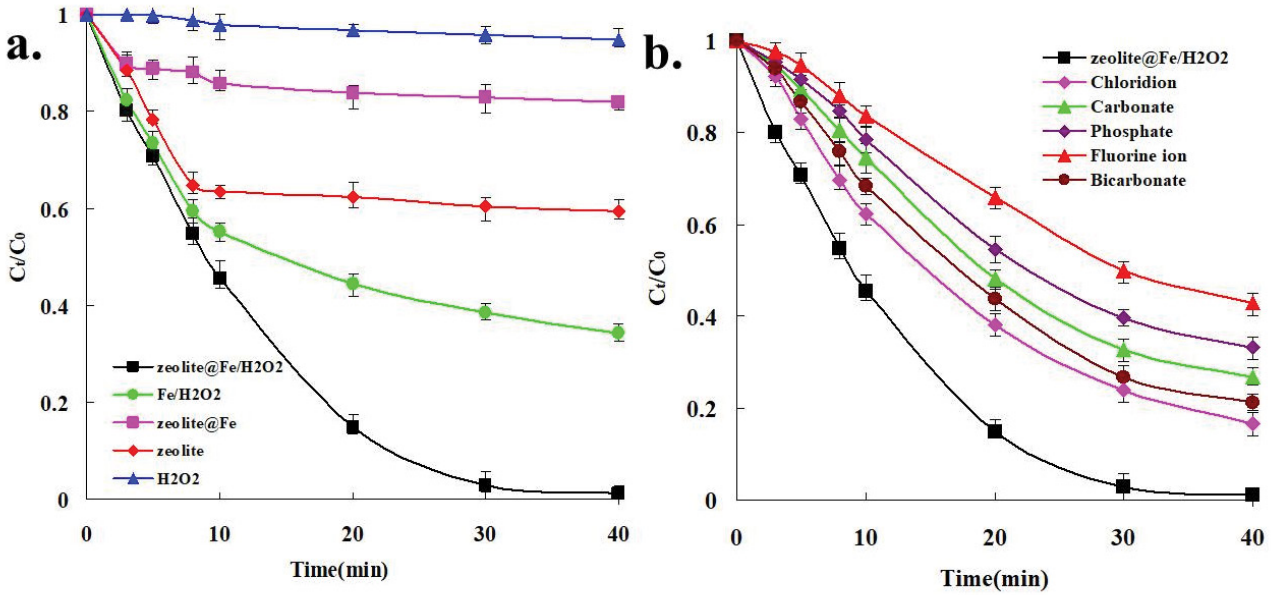

Fig. 9. Effect of solution pH on the degradation of MB in zeolite@Fe/H_2O_2 system (a) and effect of coexisting anions on the degradation of MB in zeolite@Fe/H_2O_2 system (b).

below 30°C. While if the temperature was too high, it was not favorable to the practical industrial application, and the solution would be boiled in the process of reaction. It could be seen from Fig. 10a that at a reaction temperature of 60°C, the degradation efficiencies of MB in zeolite@Fe/H_2O_2 system was the best, with a residual rate of 0.03 at 10 min. When the reaction time was 20 min, the residual rate of pollutant was greatly decreased to 0.001, and the MB was almost completely degraded. In addition, when the reaction temperature was 50°C, the residual rate of MB was 0.003 at 60 min. Also, the residual rate was 0.005 at 80 min as the reaction temperature was 40°C. Moreover, the removal rate of pollutant was the worst when the temperature was 30°C, and the residual rate was still 0.098 at the reaction time of 100 min. These findings suggested that the increase of reaction temperature could promote the progress of Fenton-like reaction, which was consistent with the results of other researchers [47,78,79]. At present, there are generally two views on the influence of temperature on Fenton-like reaction. The first is that the increase of temperature will accelerate the decomposition of H_2O_2 into H_2O and O_2, which contribute to the increase of degradation efficiencies [80]. Another view is that the appropriate increase of temperature can promote the formation of •OH radical, which can promote the reaction process [81]. Currently, most researchers have found that when the temperature is less than 60°C, the rate of Fenton-like reaction often increases with the higher temperature [78–81]. This would suggest in this temperature range (<60°C), the promotion effect of temperature rises on the formation of •OH radical should be greater than that of H_2O_2 decomposition.

During the process of industrial organic wastewater treatment, considering the limited residence time of wastewater in the reactor and excessively energy and cost consumption caused by high reaction temperature, more economical reaction temperature should be maintained from 40°C to 50°C [47,79]. Besides, changes of UV absorption spectra under visible light for MB at different reaction time are shown in Fig. 10b. It was certain that MB peaks were decreased with the reaction time gradually, which stated that MB displayed favorable Fenton-like degradation performance in zeolite@Fe/H_2O_2 system.

In this research, the first-order and the second-order reaction kinetic equations were used to investigate the reaction process of zeolite@Fe/H_2O_2 system, and the experimental data was obtained from the degradation of MB within the first 30 min (Fig. 10a), and the fitting results are depicted in Fig. 10c and d. The first-order reaction kinetic equation [82] was as follows:

$$\ln\frac{C_t}{C_0} = k_t \tag{1}$$

where C_0 and C_t were the concentration of pollutant at the beginning of degradation and at the degradation time of t, and k (min^{-1}) was the first-order rate constant.

The second-order reaction equation [83] is as follows:

$$\frac{1}{C_t} - \frac{1}{C_0} = k_t \tag{2}$$

where C_0 and C_t were the concentration of pollutant at the beginning of degradation and at the degradation time of t, and k (min^{-1}) was the second-order rate constant.

The Arrhenius equation [84] [Eq. (3)] was often used to analyze the effect of temperature on the reaction rate constant and calculate the reaction activation energy.

$$\ln k = \frac{-E_a}{RT} + \ln A \tag{3}$$

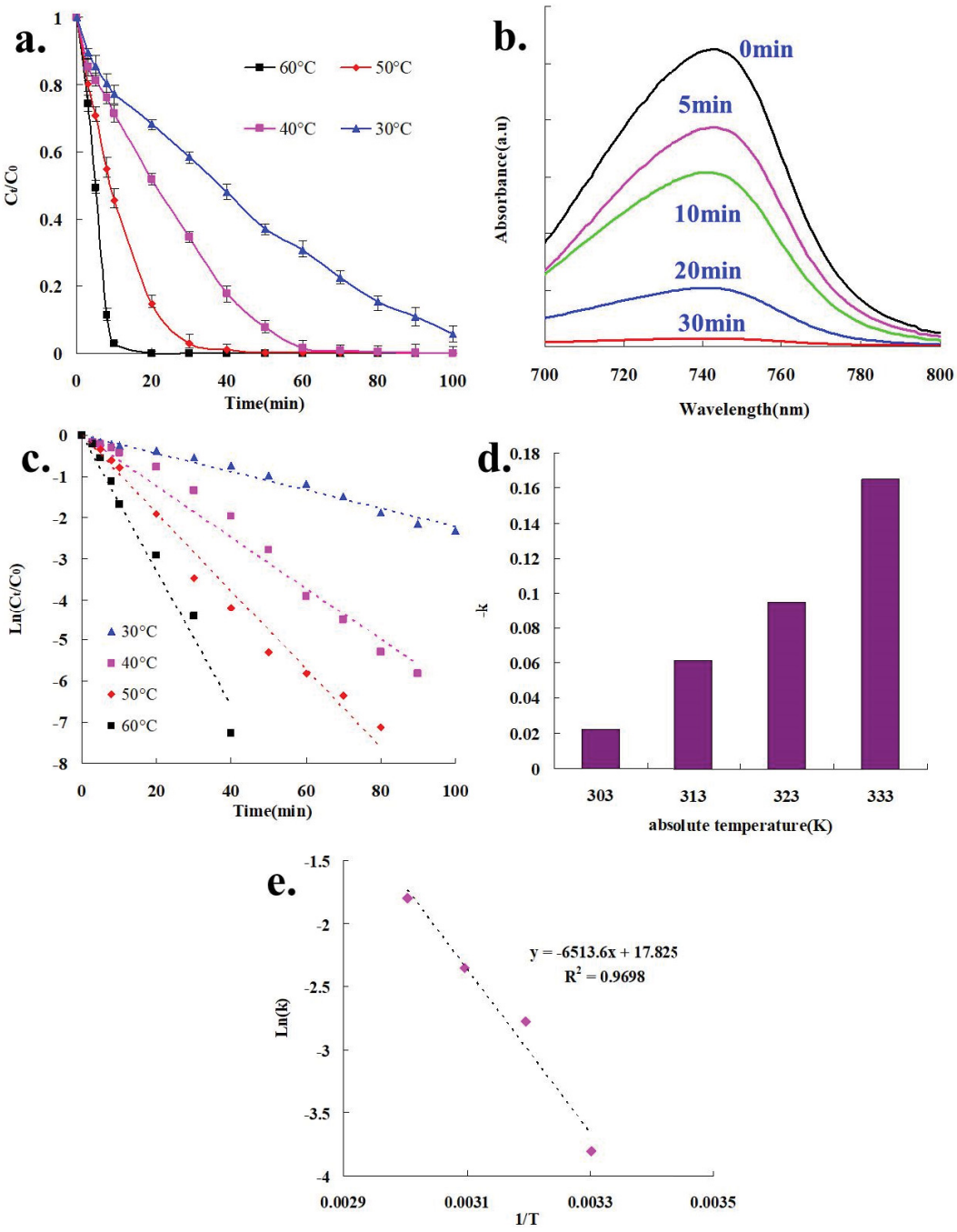

Fig. 10. Effects of temperature and reaction time on the degradation of MB in zeolite@Fe/H_2O_2 system (a), absorption spectra of UV-visible for MB solution degraded by zeolite@Fe/H_2O_2 system (b), apparent fitting findings using the first-order model (c), constants of first-order reactions for MB degradation (d) and Arrhenius equation analysis plot (e).

where k (min^{-1}) was the first-order rate constant of reaction; E_a (J mol^{-1}) is the apparent reaction activation energy; A is preexponential factor; R (8.314 J mol^{-1} K^{-1}) is gas constant; T(K) is absolute temperature.

The related fitting results calculated by the first-order and the second-order reaction kinetic equations are displayed in Tables 1 and 2, respectively. Combined the fitting findings of Fig. 10c and d with the related fitting results of Tables 1 and 2, it was presented that the first-order reaction kinetics equation was better to describe the degradation process of MB in zeolite@Fe/H_2O_2 system at different reaction temperatures compared with the second-order reaction kinetics. Besides, the fitting values of R^2 for the first-order reaction kinetics equation at different temperatures were all above 0.97, while the R^2 value of the second-order reaction kinetics equation were significantly lower. In addition, it

Table 1
The first-order rate constants calculated from experiment data (zeolite@Fe/H_2O_2 system)

Temperature (°C)	k (min^{-1})	R^2
30	0.0223	0.9833
40	0.0622	0.9783
50	0.0953	0.9840
60	0.1649	0.9761

Table 2
The second-order rate constants calculated from experiment data (zeolite@Fe/H_2O_2 system)

Temperature (°C)	k ($L\ mg^{-1}\ min^{-1}$)	R^2
30	0.0034	0.8179
40	0.0983	0.5919
50	0.4201	0.6310
60	0.9682	0.4953

was seen that the reaction rate constants of k were increased with the rise of temperature in both the first-order and the second-order reaction kinetics, suggesting that the reaction process in Fenton-like system was faster with a higher temperature. In this research, it could be concluded that the first-order reaction kinetics was more suitable for describing the reaction process of MB in zeolite@Fe/H_2O_2 system. The data of the first-order kinetic analysis were used to analyze the activation energy of the reaction, and the results are shown in Fig. 10e. It could be seen that the value of R^2 was 0.9698, and the apparent reaction activation energy of zeolite@Fe/H_2O_2 system was 54.15 kJ mol^{-1}. Table 3 lists some recent research findings on the degradation of MB by Fenton-like reactions. It could be seen that many Fe containing materials efficiently degraded MB under Fenton-like reaction system. Considering various reaction conditions (including catalyst dosage, MB concentration, H_2O_2 concentration, reaction time, temperature and pH value), zeolite@Fe in this study should be a Fenton-like catalyst material with excellent degradation efficiency for MB.

3.9. Stability and reusability of the zeolite@Fe

The stability of catalytic performance was crucial for catalytic materials. The durability and stability of zeolite@Fe was evaluated through the repeated usage of composite catalyst for four times to degrade MB. The SEM, XRD and XPS analysis were also conducted to characterize the recycled zeolite@Fe catalytic material after 4th reaction, as presented in Fig. 11. It was seen that the morphology of catalyst after 4th degradation experiment remained nearly the same as the original one. Besides, the main XRD peaks of zeolite@Fe after 4th reaction still could be observed. The results suggested that the structural integrity of catalyst material almost maintained the same after the recycling usage.

Fig. S1 showed the XPS analysis results of zeolite@Fe after 4th reaction. It is observed from Fig. S1a that the main

Table 3
The comparison of degradation efficiencies and conditions of MB through Fenton-like process

Type	Catalyst dosage ($g\ L^{-1}$)	Concentration of MB ($mg\ L^{-1}$)	Concentration of H_2O_2 ($mmol\ L^{-1}$)	pH	Reaction time (min)	Reaction temperature (°C)	Degradation efficiency (%)	References
Fe_3O_4 nanoparticles	0.5	30	1	3	20	25	100	[85]
$Ba_{0.4}Sr_{0.6}Fe_{12}O_{19}$	0.25	10	19	7	140	room	100	[86]
Fe-g-C_3N_4 porous nanosheets	0.2	100	199.4	7	60	room	100	[87]
Iron oxide nanoparticles	2.0	100	560	3.5	90	90	100	[88]
γ-Fe_2O_3/Biochar + UV	2.0	50	200	7	60	25	99.5	[89]
Fe_3O_4@C nanoparticles	2.0	100	30	5	180	25	100	[90]
Fe-based metal–organic frameworks	0.5	15	5.9	–	720	25	88	[91]
Fe(II)-doped g-C_3N_4	0.5	50	200	6.5	80	25	around 98	[92]
Functionalized magnetite nanoparticles	3.5	100	310	–	40	10	100	[93]
FeNi/C-30	1	30	100	7	60	25	99	[94]
Zeolite@Fe	1	20	about 388	7	50	50	98.5	This work

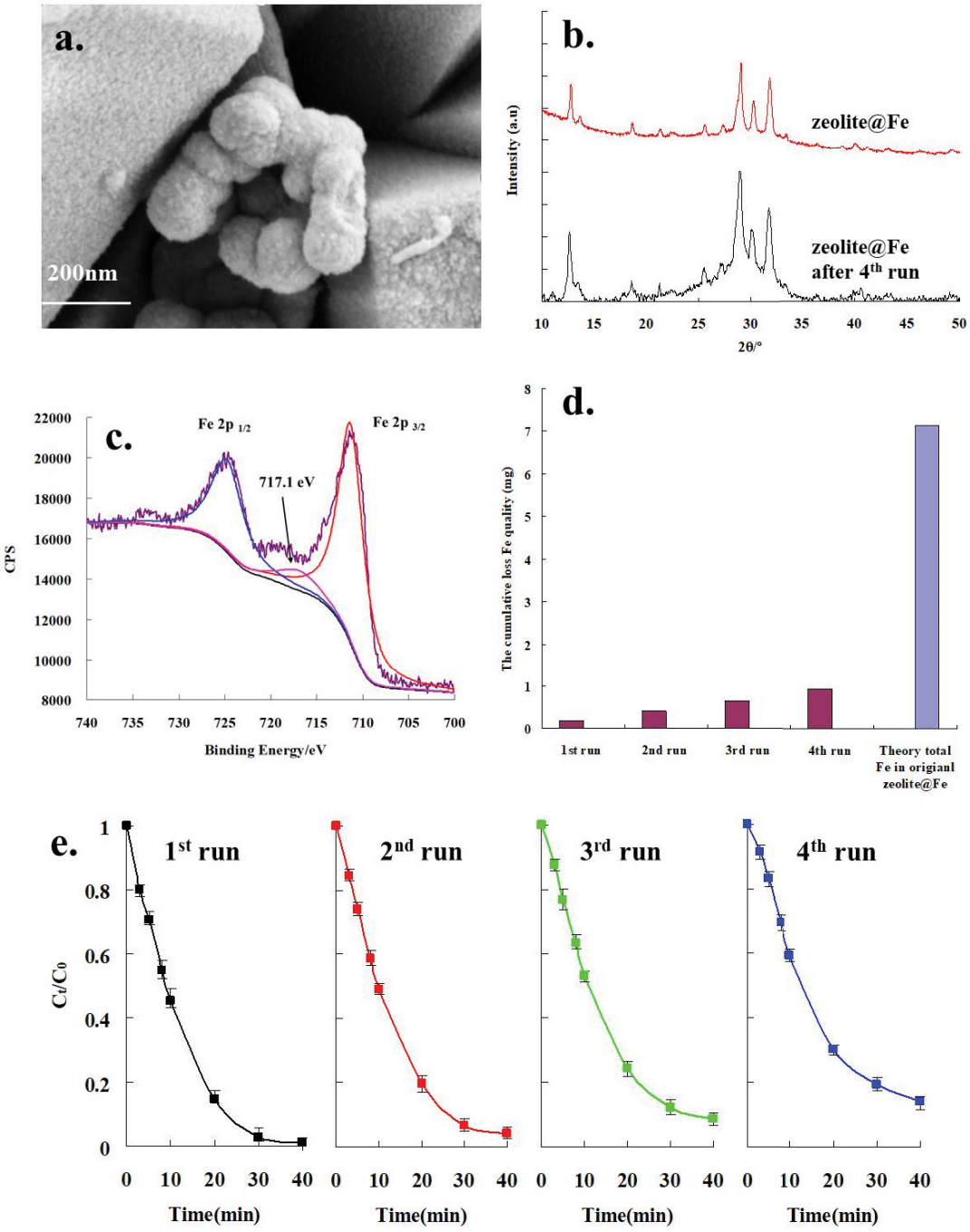

Fig. 11. (a) The morphology of catalyst after 4th reaction, (b) XRD patterns of zeolite@Fe before and after 4th reaction, (c) high-resolution XPS spectra of Fe2p zeolite@Fe after 4th reaction, (d) cumulative loss Fe quality during four reaction systems and (e) degradation curves of reusing zeolite@Fe catalyst.

peaks are Fe2s (838.2 eV), Fe2p (711.1 eV), O1s (531.1 eV), K2p (294.1 eV), C1s (285.1 eV), Si2p (101.7 eV), and Al2p (74.6 eV), respectively, and all the constituent elements could be found in original zeolite@Fe material. The chemical composition gained from XPS was as follow: Al (15.3%), Si (14.8%), K (6.5%), Fe (2.42%), and O (61.1%). Combined with the content of Fe (2.8%) in original zeolite@Fe, the loss rate of Fe element after 4 cycles was about 13.6%, which indicated that the zeolite@Fe catalyst remained basically stable. Also, the high-resolution XPS spectra of Al2p and Si2p for zeolite@Fe after 4th reaction are shown in Fig. S1b and c, respectively. Both the Al2p and Si2p spectra could be decomposed into two individual peaks (74.3 and 74.7 eV) and (100.9 and 101.8 eV) after the peak fitting. Combined

with previous analysis of Fig. 7, the appearance of new peaks at about 74.7 and 100.9 eV came from the adsorption of Fe into zeolite structure, so the relative decreasing of peaks intensities at 74.7 and 100.9 eV implied that part of adsorbed Fe element was lost during four cycles of Fenton-like reaction process. Simultaneously, the O1s peaks (Fig. S2d) could also be divided into three curves at 529.4, 531.2, and 532.8 eV, respectively. Furthermore, the high-resolution XPS spectrum of Fe2p of zeolite@Fe after 4th reaction is shown in Fig. 11c. As Fig. 11c shows, two strong peaks around binding energies of 725.1 eV ($Fe2p_{1/2}$), 711.21 eV ($Fe2p_{2/3}$) and a shoulder satellite peak at around 717.3 eV still could be found, which indicated that Fe element in zeolite@Fe maintained the state of trivalent iron after four cycles of reaction process.

Fig. 11d shows the concentration of Fe dissolved in reaction systems. The synthesis of zeolite@Fe was realized through the adsorption process of Fe element on zeolite. Due to the restriction of adsorption/desorption equilibrium, when there was no Fe element in the solution, minority Fe element adsorbed on zeolite would tend to be re-desorbed into the solution. In this case, it was observed that in each degradation system, the concentration of Fe element was about 1.3, 1.6, 1.73 and 2.1 mg L^{-1}. This result was higher than that of other researchers [95,96]. After the calculation, the total Fe dissolved of four cycles was about 0.673 mg, and this quality was much lower than about 7.13 mg (theoretically, all the Fe element contained in 0.1 g of zeolite@Fe catalyst based on the XPS results of Fig. 7) and the total loss rate of Fe element was about 9.41%, which also indicated that zeolite@Fe remained basically stable during the reaction process. According to the results of other researchers, the leaching of Fe will lead to the traditional homogeneous Fenton reaction process in the reaction system, so as to promote the degradation of pollutants in single degradation experiment [95]. However, in this study, due to the steps of filtration, washing and drying process in the catalyst recycle, it would lead to the structure destroy of catalyst and the loss of total Fe elements in the recycle reaction system, which might further reduce the pollutant removal efficiency. Furthermore, as depicted in Fig. 11e, about 10.8% of MB removal efficiency was decreased after 4th recycle reaction. All these findings indicated zeolite@Fe as a heterogeneous catalyst was mainly stable in zeolite@Fe/H_2O_2 system.

Furthermore, EDX line and Element mapping analysis were applied for zeolite@Fe after 4th recycle reaction and the results are shown in Fig. 12. It can be seen from Fig. 12a and b that all elements including Al, Si, O, K, and Fe were still distributed on the energy spectrum analysis line (about 10 μm). Whereas, the CPS strengths of Fe were much lower than that of zeolite@Fe (Fig. 5b). Similar results could be obtained from the element mapping analysis (from Fig. 12c–g). Compared with zeolite@Fe (from Fig. 5c–g), it could be appeared that the distribution intensity of Fe changed to much dull and loose. The total chemical content (atomic percentage/%) of element in analysis line was as follows: Al (15.5%), Si (15.1%), K (6.5%), Fe (1.8%), and O (60.9%). Compared with the EDX results of the original zeolite@Fe, the total loss rate of Fe element was about 14.2%. All the results of EDX, XPS and Fe dissolved after 4th cycles indicated that about 10% of Fe would be lost. The decrease of Fe content implied the loss of Fe element during the Fenton-like reaction, which might be one of the reasons for the decreasing of recycle degradation

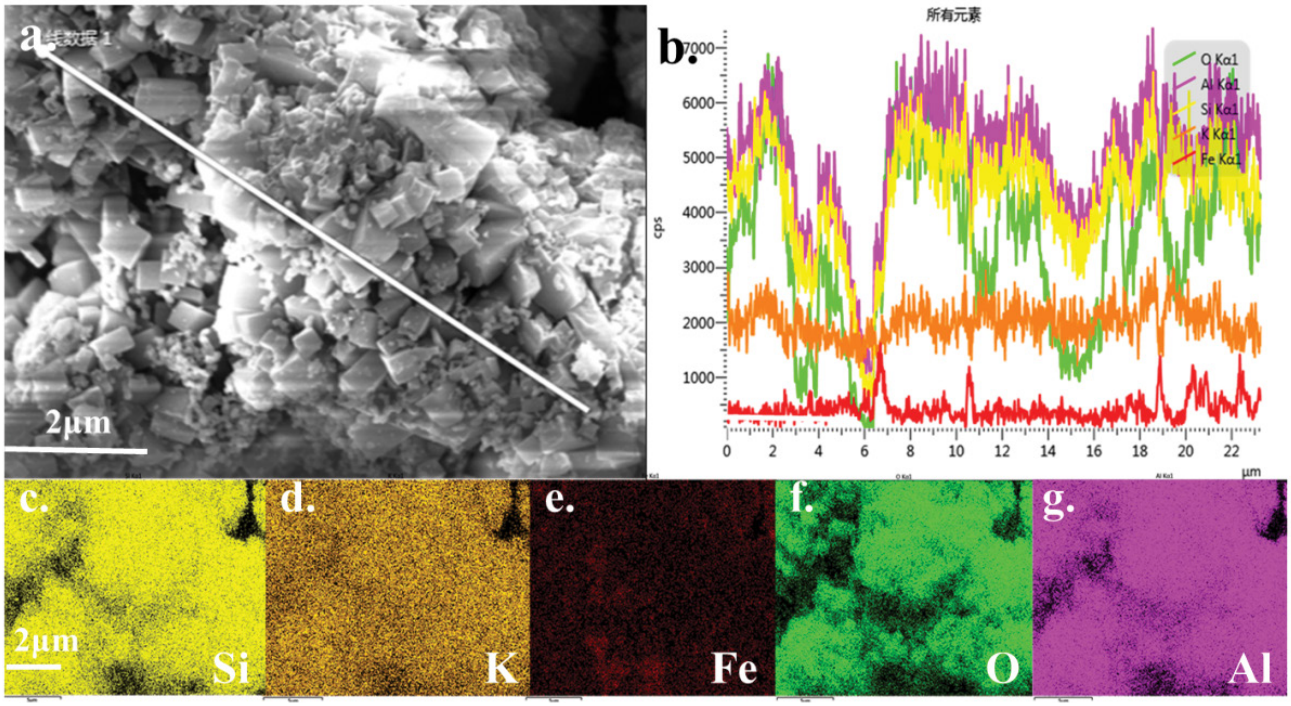

Fig. 12. EDX line and element mapping analysis results of zeolite@Fe after 4th reaction.

efficiencies for the target pollutant. In the comprehensive sewage discharge standard, there was no restriction on Fe concentration, while the presence of Fe would affect the chromaticity index of wastewater. In the environmental quality standards of surface water environment, the standard for supplementary items of centralized drinking water surface water sources was limited to 0.3 mg L^{-1}. In this case, the leaching of Fe element did have a certain impact on the water environment. Accordingly, we investigated the method of reducing Fe element in the treated water by supplementing a certain amount of new original zeolite after the photocatalytic treatment was completed. The results showed that Fe element in the treated aqueous solution could be reduced to less than 0.3 mg L^{-1}, and the catalytic performance of the reused material maintained stable (the findings were shown in supporting information S2).

3.10. Potential degradation mechanisms in zeolite@Fe/H_2O_2 system

Generally speaking, the degradation of pollutants by Fenton-like reactions was mainly based on various free radicals generated during the reaction. It was believed that hydroxyl radical was the major reactive radicals in Fenton-like system [97–99]. To illustrate the potential degradation mechanism and the active species that played a major role in Fenton-like reaction system, the radical capture agents were added in the reaction process, while FFA was considered to be the capturing agent of $^{\bullet}O_2$ and $^{\bullet}OH$ [96], benzoquinone was used as the capturing agent of $^{\bullet}O_2$, and TBA, IPA and EtOH was utilized as the capturing agent of $^{\bullet}OH$ [100,101]. The related results are displayed in Fig. 13. It could be seen that the addition of FFA greatly reduced the degradation efficiency. The kinetic reaction constant decreased from 0.1051(no agents) to 0.0027 (FFA), which indicated that both $^{\bullet}O_2$ and $^{\bullet}OH$ played an important role in the reaction process. Meanwhile, the effect of BQ on the degradation effect was significantly less than that of TBA, IPA, and EtOH. In addition, the kinetic reaction constant of BQ, TBA, IPA, and EtOH was 0.0245, 0.0042, 0.0097, and 0.0134, respectively. The result implied that the role of $^{\bullet}OH$ was significantly greater than that of $^{\bullet}O_2$ in the reaction process. Also, $^{\bullet}OH$ should be the free radical that played a major role in the reaction process.

ESR technology could help us effectively capture the reactive free radicals generated during the reaction process, as presented in Fig. 14a and b. It is seen from Fig. 14a that there is no signal of $^{\bullet}OH$ appeared when only zeolite@

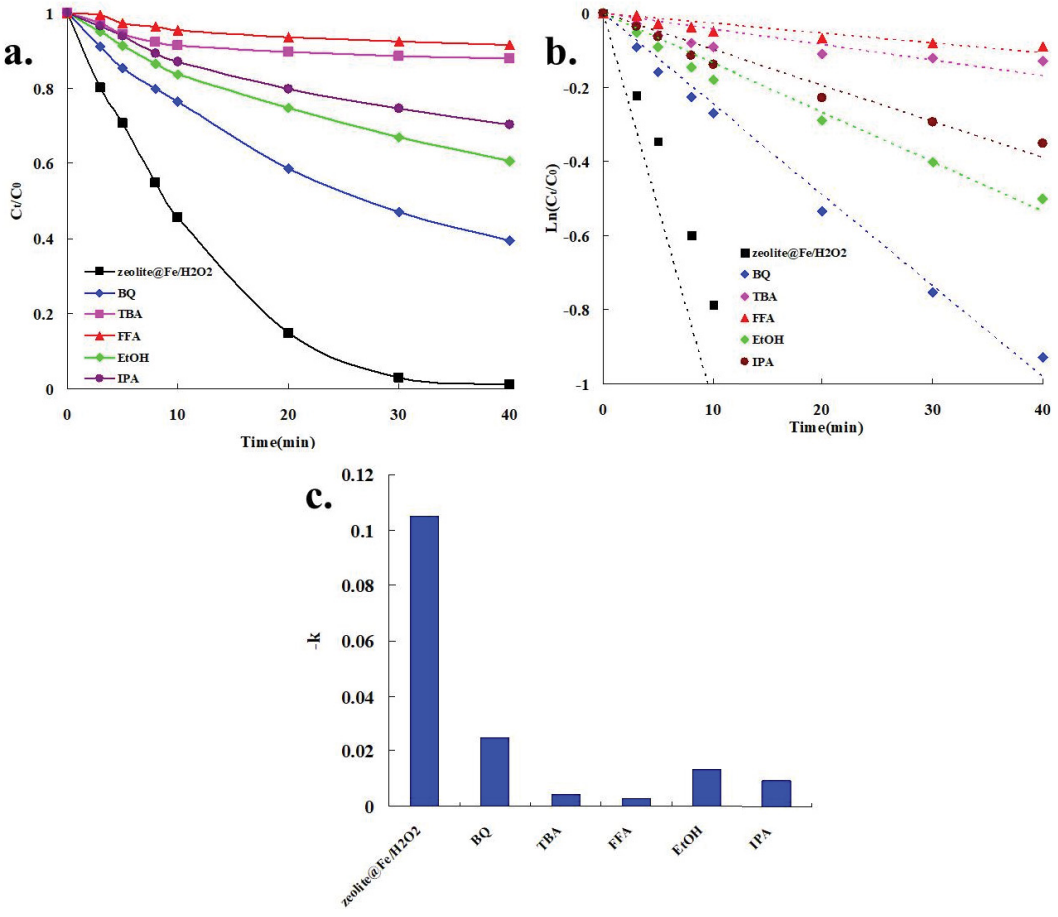

Fig. 13. Effect of free radical trapping agents on the degradation of MB in zeolite@Fe/H_2O_2 system (a), apparent fitting findings using the first-order model (b), and constants of first-order reactions for the effect of free radical trapping agent (c).

Fe exited in the reaction system, indicating there was no formation of •OH in this reaction system. When both zeolite@Fe and H_2O_2 existing in the reaction system, a typical characteristic peak of •OH (1:2:2:1) appeared in the ESR spectrum [77,102]. This suggested that •OH appeared in the reaction system of zeolite@Fe/H_2O_2, and similar results could also be obtained from Fig. 14b. There was no $•O_2^-$ in individual zeolite@Fe reaction system, but $•O_2^-$ was appeared in zeolite@Fe/H_2O_2 reaction system [102,103]. Such findings indicated that in Fenton-like zeolite@Fe/H_2O_2 reaction system, •OH and $•O_2^-$ should be the main mechanism for the degradation of organic pollutant. Meanwhile, the intensity of the characteristic curves of •OH was greater than that of $•O_2^-$ by comparing Fig. 14a with Fig. 14b. This suggested that in the reaction system, the concentration of •OH was greater than that of $•O_2^-$, so the degradation effect of •OH on pollutants might be stronger than that of $•O_2^-$, which was consistent with the result of Fig. 13a.

The DFT theoretical calculations could analyze the active sites, paths and intermediate products of the catalytic process, and then analyzed the mechanism of the entire catalytic reaction. To further analyze the reaction mechanism of zeolite@Fe material, the VASP software based on DFT calculation method was used to investigate the reaction process of zeolite@Fe materials. Fig. 15a and b display the theoretical structure models of zeolite and zeolite@Fe. It is observed from Fig. 15a that as a kind of typical aluminosilicate material, zeolite was constructed with silicon-oxygen tetrahedron and aluminum-oxygen tetrahedron as basic units. Besides, the basic tetrahedral structures were regularly connected in a common oxygen element. At the same time, the K elements were regularly arranged in the gaps of the structure. Moreover, the crystal structure parameters of the theoretical model were a = 9.9041 Å, b = 9.9041 Å, c = 13.090 Å, $\alpha = 90.00°$, $\beta = 90.00°$, and $\gamma = 90.00°$. Meanwhile, the Space group name was I, which was very close to the crystal structure parameters of the PDF#38-0216 ($KAlSiO_4$) mineral in the standard mineral card. In previous experimental results, we found that part of K element in zeolite material was replaced by Fe element after the adsorption was occurred. Hence, we replaced parts of K element in the theoretical structure of zeolite with Fe element to simulate the theoretical model of zeolite@Fe, as presented in Fig. 15b. In addition, Fig. 15c and d show the comparison findings between the calculated XRD diffraction results of the theoretical model and experimental XRD results of sample. It can be found from Fig. 15c and d that, whether the peak position of diffraction peak or the relative intensity of the peak, the XRD theoretical calculation and the actual experimental results were very similar. Accordingly, these findings proved that the theoretical model constructed was appropriate for the research.

Fig. 16 displays the theoretical model of DFT calculation (Fig. 16a and b) and the optimization result model after the structural optimization calculation (Fig. 16c and d). In this study, to fit the Fenton-like reaction process that occurred on the surface of zeolite@Fe, a surface model based on the zeolite@Fe theoretical unit cell model (Fig. 15b) were constructed. Then, we selected the (100) crystal plane of zeolite@Fe crystal model (Fig. 15b) as the theoretical catalytic surface, and constructed a 2 × 1 × 1 super cell surface structure and a 10 Å surface void layer, as seen as Fig. 16a. It was probably believed that Fe element in Fig. 16a was the catalytic active site of the Fenton-like reaction. In this case, before the theoretical calculation of DFT, we set a molecule of H_2O_2 on the top of Fe element (2 Å), and the theoretical structure is shown in Fig. 16b. Fig. 16c and d show the DFT calculation results based on VASP software. It was observed that after the calculation of DFT, both the O–O bond and O–H bond in H_2O_2 molecule were separated to form a free OH group and H group, and the remaining O were captured by Fe element in the surface model to form the Fe–O group, and a deeply analysis can be obtained from Fig. 17.

Fig. 17 describes the charge density distribution at 0.75d of the (0 1 0) section of the model in Fig. 16a–c. It is clearly observed from Fig. 17a that the charge distribution of Fe element site was relatively strong. After H_2O_2 molecules were added, the charge distribution of H_2O_2 molecules can be clearly observed in Fig. 17b, and did not overlap the charge

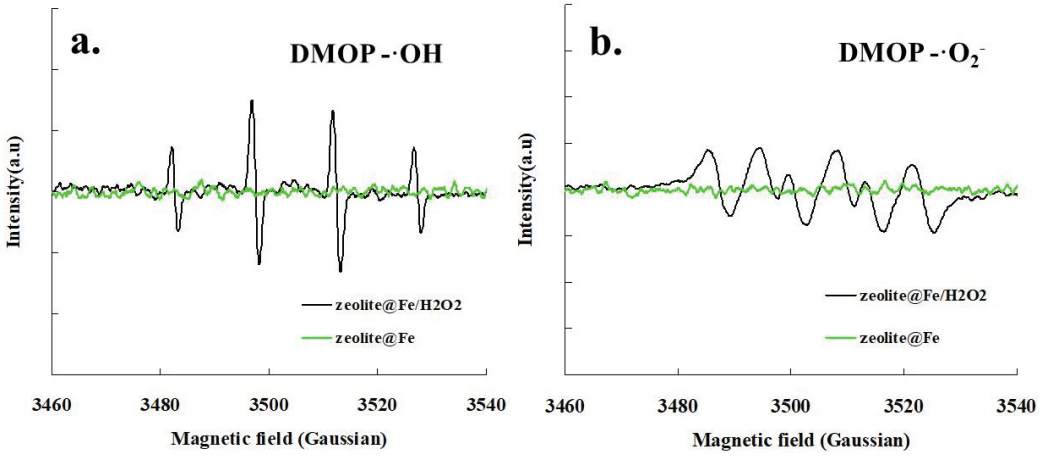

Fig. 14. ESR spectra of radical adducts trapped by DMPO in zeolite@Fe/H_2O_2 and zeolite@Fe reaction systems (a) and ESR spectra of radical adducts trapped by DMPO in zeolite@Fe/H_2O_2 and zeolite@Fe reaction systems (b).

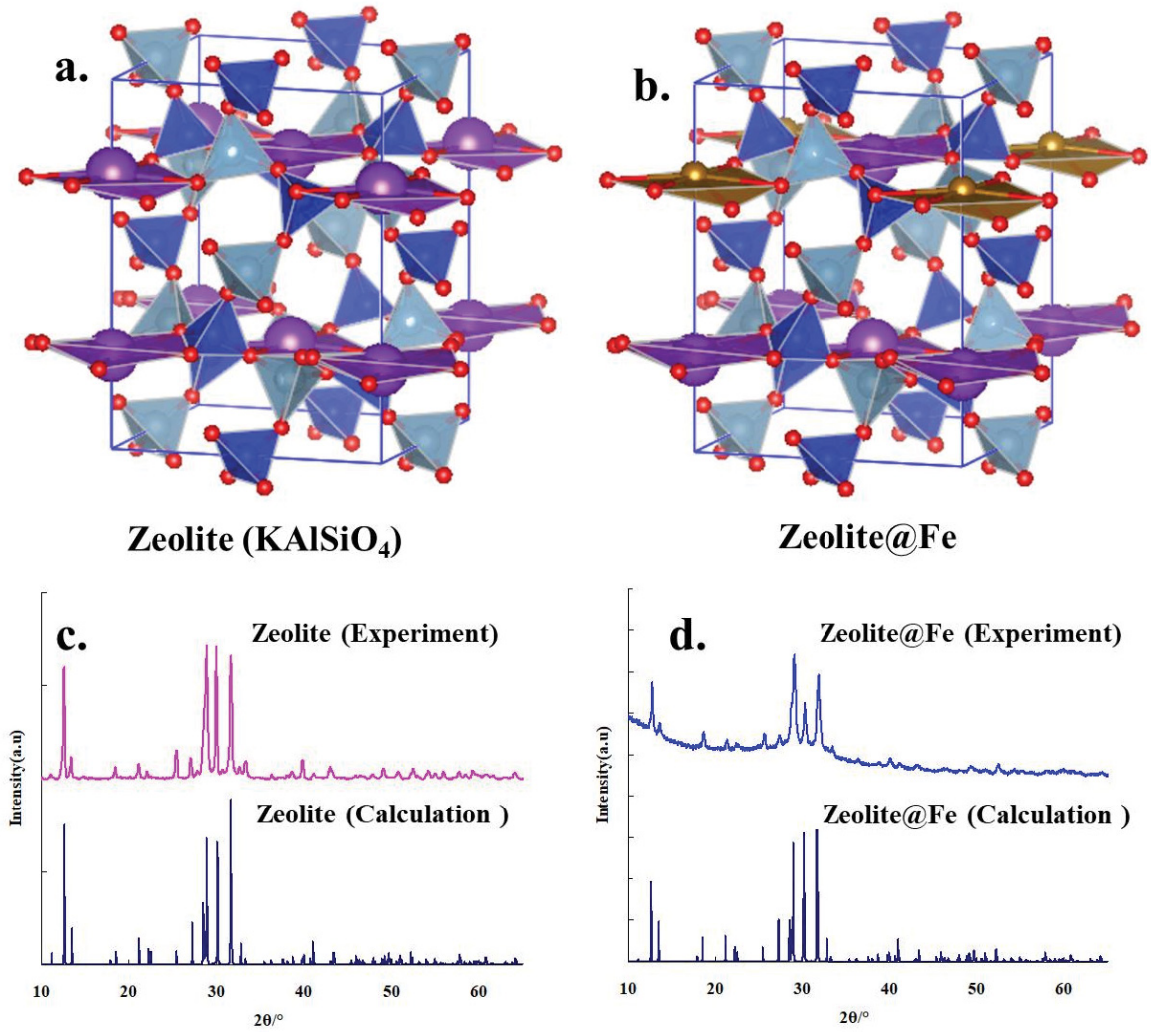

Fig. 15. Theoretical structure model of zeolite (a) and zeolite@Fe (b) (red ball is O atom, violet ball is K atom, blue ball is Si atom, blue grey ball is Al atom, brown yellow ball is Fe atom); Comparison between theoretical model XRD calculation results and actual sample XRD analysis results (c and d).

distribution of Fe elements. In addition, after the DFT calculation was completed, the charge analysis of the H_2O_2 molecule was split (as shown as Fig. 17c), and the charge distribution of the OH group appeared on the upper parts, while the charge distribution of the remaining O in the lower parts was overlapped with the charge distribution of Fe element in the surface model. Such charge distribution results indicated that H_2O_2 molecules could not exist stably near Fe element catalytic active site in zeolite@Fe theoretically. When H_2O_2 molecules were close to Fe elements catalytic active site, Fe active sites on the surface of zeolite@Fe was able to tear H_2O_2 molecules apart, forming a free OH group and H group while capturing one O element after complex interactions between them.

To further study the reaction process between Fe–O group and H_2O_2 molecules, we deleted the H group and OH group in the first step of DFT calculation results (Fig. 16c), and added H_2O_2 molecules again to construct the theoretical composite catalytic structure-2, as described in Fig. 18a, and the results after the DFT calculation are shown in Fig. 18b and c. It is observed from Fig. 18b and c that the O–O bond and O–H bond in the H_2O_2 molecule were separated again to form a free OH group and H group. Meanwhile, one remaining O in the H_2O_2 molecule combined with the O captured by Fe element in the surface model to form O_2 molecule and got rid of the constraints of the surface model. Fig. 19 shows the charge density distribution at 0.75 d of the (0 1 0) section of the model in Fig. 17a and b. The charge distributions of Fe–O group and H_2O_2 molecules can be clearly observed in Fig. 19a, and the two distributions had no overlay. When the DFT calculation was completed, the charge analysis of the H_2O_2 molecule separated (Fig. 19b), and the charge distribution of the OH group appeared again on the upper part, and the charge distribution of O_2 molecule appeared on the lower part and did not overlap the charge distribution of Fe surface model. These findings suggested that when another H_2O_2 molecule approaching to the catalytic active site of Fe captured O (Fig. 19a), the

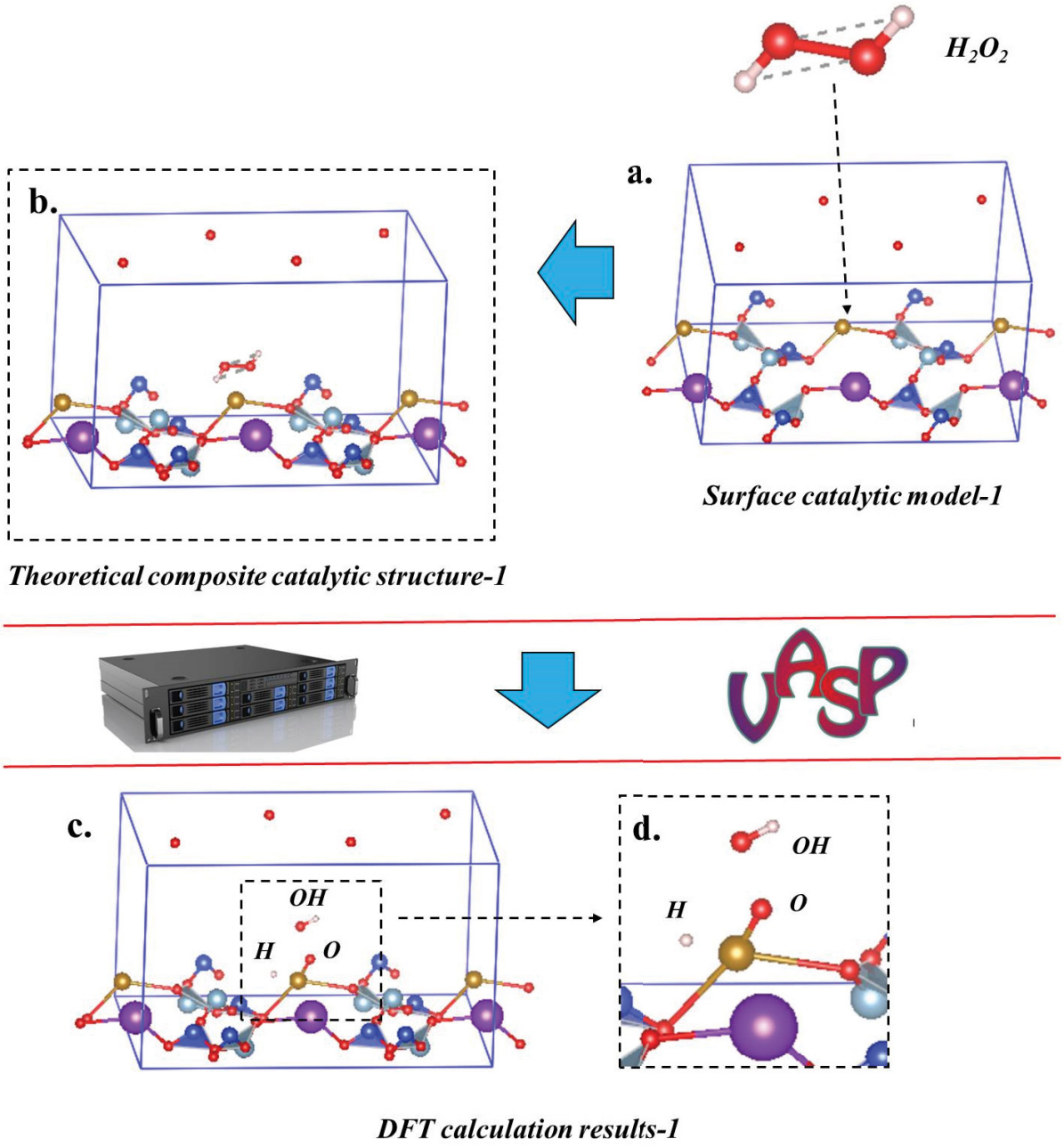

Fig. 16. DFT catalyst calculation process and the results of stage one.

H_2O_2 molecule would be torn again, and the newly generated O would combine with the O previously captured by Fe element catalytic sites, forming free O_2 molecules and getting rid of the constraints of Fe catalytic sites. At this time, the theoretical surface catalytic structure of zeolite@Fe returned to the initial state.

Based on the above theoretical calculation results, we speculated that when the reaction was carried out in liquid phase, a large amount of free OH groups would form considerable •OH radicals. Such •OH species could react with the target pollutant in the reaction system to achieve the purpose of degrading pollutant (as shown in Fig. 20). Hence, •OH radicals might be one of the main mechanism of zeolite@Fe Fenton-like reaction system to degrade pollutant, which was consistent with the results of •OH radical capturing experiments and ESR spectra results in Fig. 14. The H group formed at the same time would react with other substances in the liquid phase to lose e and form H^+. In the presence of O_2 molecules in solution, the H group would react with O_2 molecule to form a certain amount of $•O_2^-$ radicals. The $•O_2^-$ radicals also had a certain degree of degradation ability to the pollutants in liquid phase, that was also consistent with the results of the $•O_2^-$ radicals capturing experiment and ESR spectra results in Fig. 14.

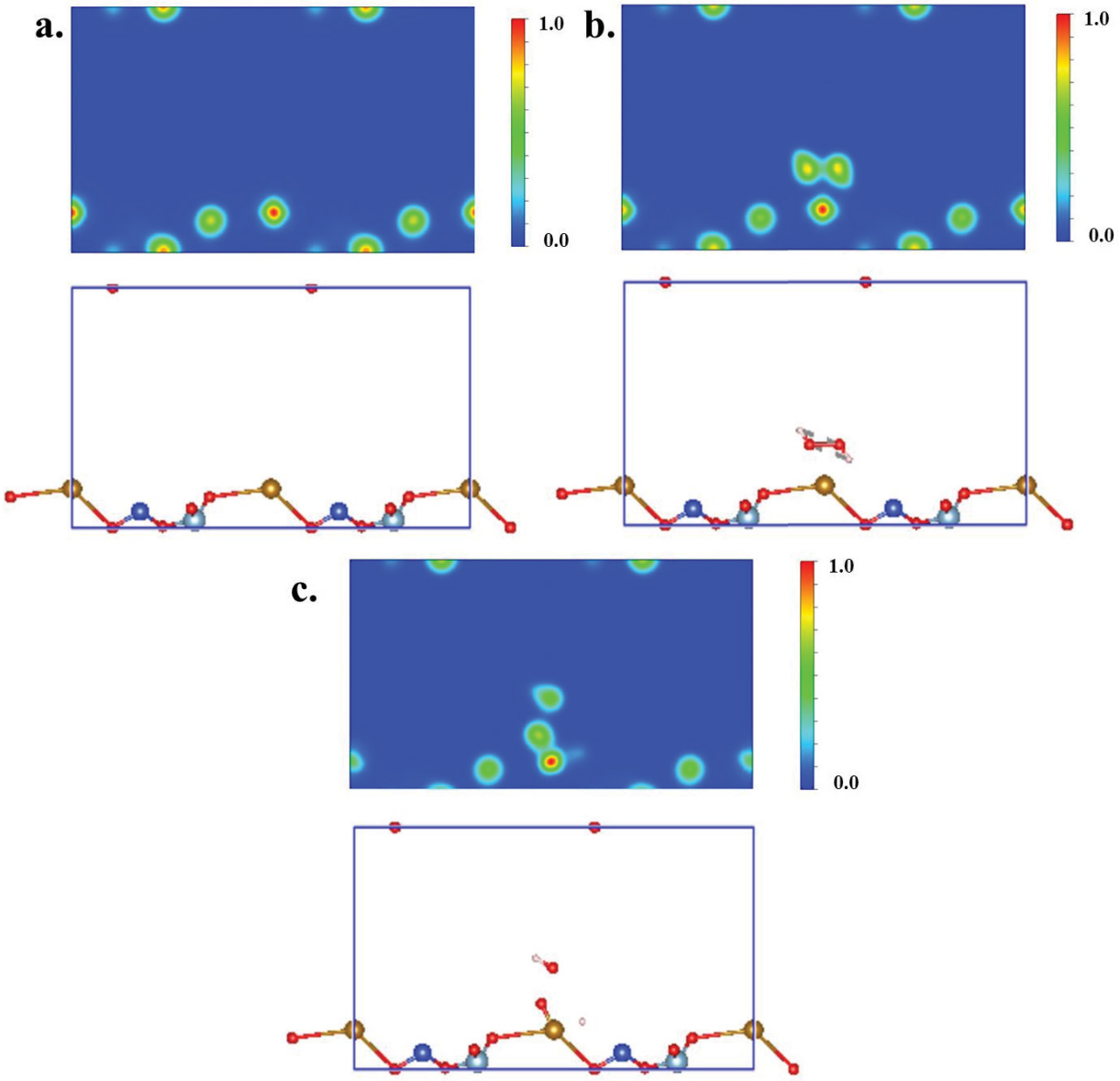

Fig. 17. Charge density distribution of theoretical structure model of Fig. 14a (a), Fig. 14b (b) and Fig. 14c (c) (0 1 0 layer, distance from origin is 0.75 d).

4. Conclusion

A novel nano-scale zeolite encapsulated with iron ions (zeolite@Fe) was successfully achieved in this research. The zeolite@Fe material was characterized by many advanced instruments, including XRD, FT-IR, SEM-EDX, and XPS, to analyze its microscopic morphology and chemical structure. In addition, the synthesized material (zeolite@Fe) was utilized as a heterogeneous Fenton-like reaction catalyst to degrade MB in the zeolite@Fe/H_2O_2 reaction. The reaction mechanism was also attempted to illustrate through the theoretical structure model and the charge density distribution of zeolite@Fe conducting by VASP software and DFT computation. The characterization results indicated that Fe^{3+} rich nano spherical-like shape material was formed on the surface of zeolite, and zeolite@Fe catalytic material was believed to be successfully achieved. Besides, there was almost no change of the chemical bonds and basic structure between original zeolite and zeolite@Fe catalyst. In the degradation experiments of MB, the addition of zeolite@Fe and H_2O_2 simultaneously greatly enhanced the degradation efficiencies compared with that of single zeolite, single H_2O_2, and zeolite@Fe, respectively. In the range of pH values from 5 to 8, zeolite@Fe/H_2O_2 reaction system could be achieved. The temperature and time had obvious effect on the degradation of MB in Fenton-like reaction system, and the first-order reaction kinetics equation could be suitably fitted the reaction process. Moreover, through the morphology and experiments findings, it was

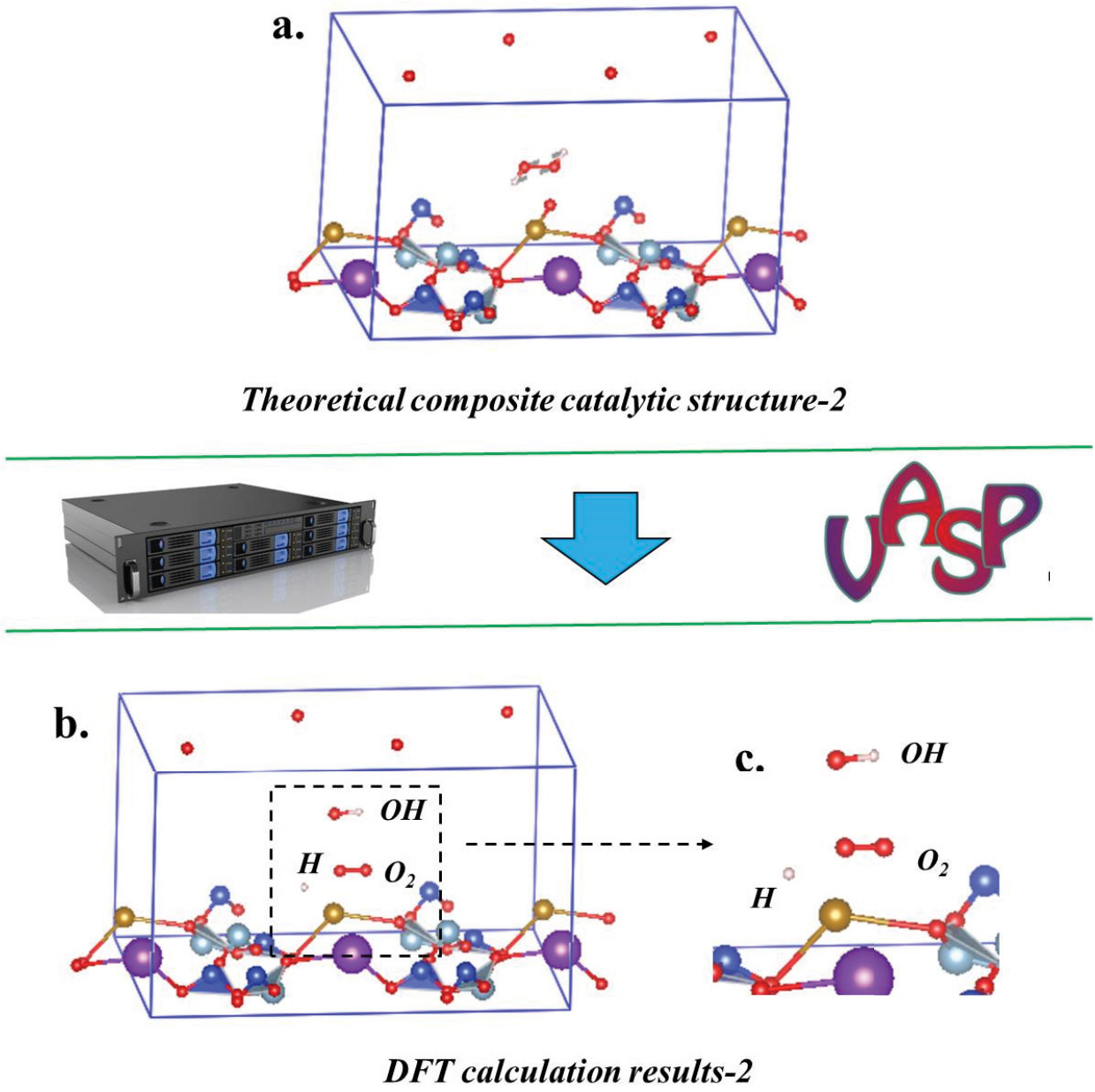

Fig. 18. DFT catalyst calculation process and results of stage two.

found that zeolite@Fe catalyst displayed relatively stable after four times of recycle usage. Additionally, the DFT calculation results of theoretical structure and surface model for zeolite@Fe stated that, the •OH radicals formed by a large amount of free OH groups were the main active species in reaction process, and they were probably one of the main factors responsible for organics degradation in Fenton-like reaction system. Furthermore, the charge density distribution analysis indicated that H_2O_2 molecules could not exist stably near Fe catalytic active site in zeolite@Fe theoretically, while after the complex close interactions between them, Fe active sites on the surface of zeolite@Fe was able to tear H_2O_2 molecules apart and form a free OH group and H group, and then produce considerable •OH radicals using to degrade the target pollutant.

Acknowledgements

This work is supported by Zhenjiang City 2021 key research and development project (Social Development) under Grant (SH2021020); 2021 Jiangsu University Students Innovation and Entrepreneurship Training Program Project (202114000015Y); Science Foundation of Jiangsu Colleges and Universities (Grant No. 17KJD610001, 17KJD610002); Jiangsu Open University School-level Scientific Research Institutions.

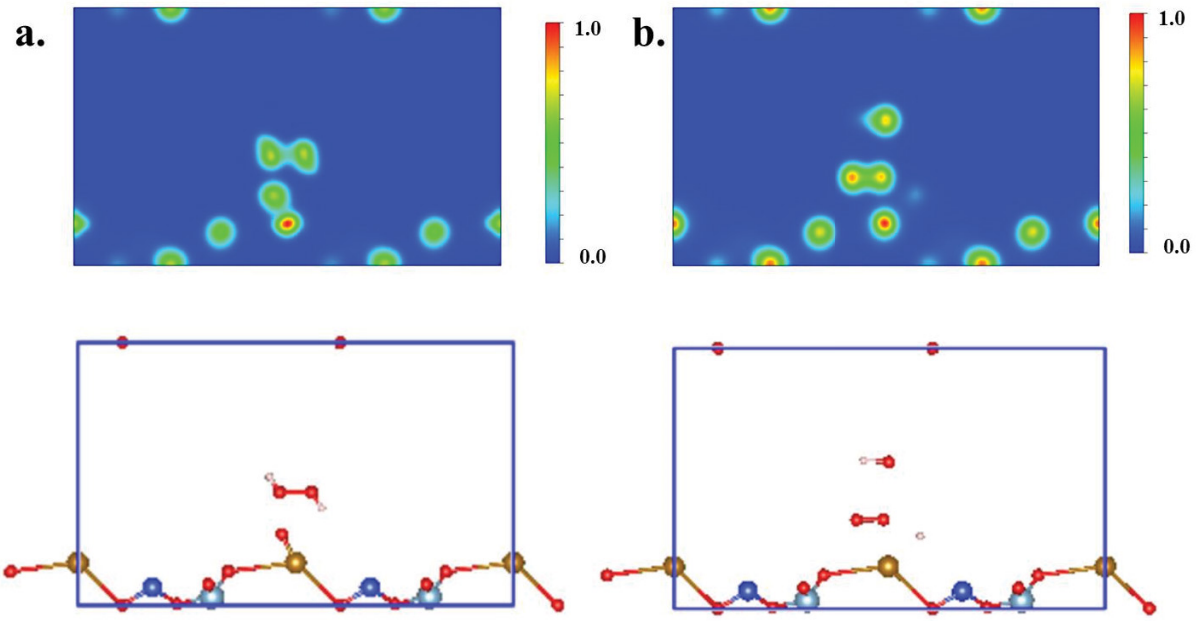

Fig. 19. Charge density distribution of theoretical surface structure (0 1 0 surface, distance from origin is 0.75 d) of theoretical surface structure model as Fig. 15a (a) and Fig. 15b (b).

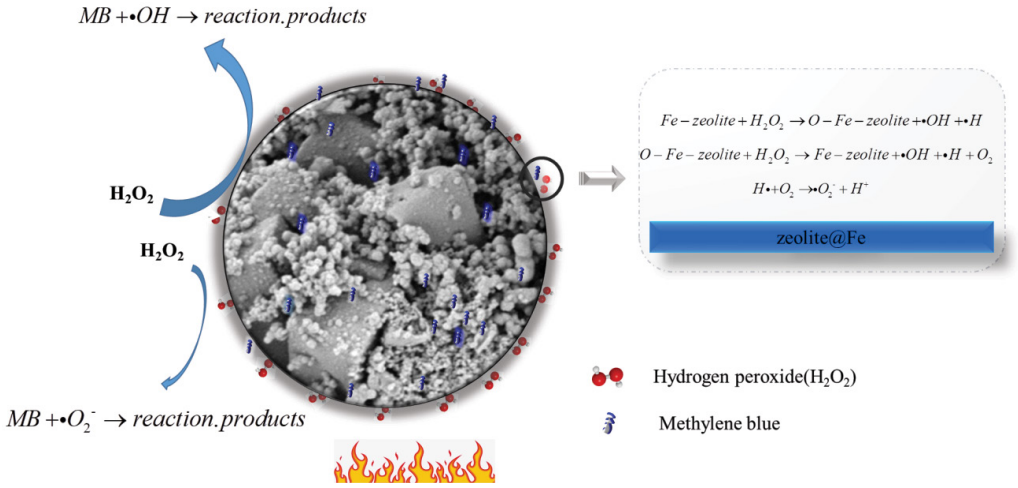

Fig. 20. Schematic diagram of the reaction mechanism of the H_2O_2 activation by zeolite@Fe/H_2O_2 system.

References

[1] Z. Kong, L. Li, Y. Xue, M. Yang, Y.-Y. Li, Challenges and prospects for the anaerobic treatment of chemical-industrial organic wastewater: a review, J. Cleaner Prod., 231 (2019) 913–927.
[2] S.N. Malik, P.C. Ghosh, A.N. Vaidya, S.N. Mudliar, Hybrid ozonation process for industrial wastewater treatment: principles and applications: a review, J. Water Process Eng., 35 (2020) 101193, doi: 10.1016/j.jwpe.2020.101193.
[3] X.Q. Pan, Z.P. Gu, W.M. Chen, Q.B. Li, Preparation of biochar and biochar composites and their application in a Fenton-like process for wastewater decontamination: a review, Sci. Total Environ., 754 (2021) 142104, doi: 10.1016/j.scitotenv.2020.142104.
[4] M. Belén Carboneras, J. Villaseñor, F. Jesús Fernández-Morales, M. Andrés Rodrigo, P. Cañizares, Biological treatment of wastewater polluted with an oxyfluorfen-based commercial herbicide, Chemosphere, 213 (2018) 244–251.
[5] A.A. Voytyuk, E.V. Moskvicheva, D.V. Shchitov, K.V. Katerinin, P.A. Sidyakin, E.Yu. Lykova, Composite-sorbent based on natural mineral and waste of biological treatment of wastewater (effluent), Key Eng. Mater., 736 (2017) 183–186.
[6] M. Makowska, M. Spychała, M. Pawlak, Efficacy and reliability of wastewater treatment technology in small meat plants, Desal. Water Treat., 221 (2021) 1–10.
[7] M. Dinari, F. Atabaki, Z. Pahnavar, R. Soltani, Adsorptive removal properties of bivalent cadmium from aqueous solution using porous poly(*N*-2-methyl-4-nitrophenyl maleimide-maleic anhydride-methyl methacrylate) terpolymers, J. Environ. Chem. Eng., 8 (2020) 104560, doi: 10.1016/j.jece.2020.104560.
[8] S.M. Huang, M.L. Hu, D. Li, L.P. Wang, C. Zhang, K. Li, Q.Q. He, Fluoride sorption from aqueous solution using

$Al(OH)_3$-modified hydroxyapatite nanosheet, Fuel, 279 (2020) 118486, doi: 10.1016/j.fuel.2020.118486.
[9] M. Bodzek, K. Konieczny, A. Kwiecińska-Mydlak, The application of nanomaterial adsorbents for the removal of impurities from water and wastewaters: a review, Desal. Water Treat., 185 (2020) 1–26.
[10] M. Corona-Bautista, A. Picos-Benítez, D. Villaseñor-Basulto, E. Bandala, J.M. Peralta-Hernández, Discoloration of azo dye Brown HT using different advanced oxidation processes, Chemosphere, 267 (2021) 129234, doi: 10.1016/j.chemosphere.2020.129234.
[11] J.W. Wang, B. Xiong, L. Miao, S.L. Wang, P.C. Xie, Z.P. Wang, J. Ma, Applying a novel advanced oxidation process of activated peracetic acid by $CoFe_2O_4$ to efficiently degrade sulfamethoxazole, Appl. Catal., B, 280 (2021) 119422, doi: 10.1016/j.apcatb.2020.119422.
[12] A. Tufail, W.E. Price, M. Mohseni, B.K. Pramanik, F.S.I. Hai, A critical review of advanced oxidation processes for emerging trace organic contaminant degradation: mechanisms, factors, degradation products, and effluent toxicity, J. Water Process Eng., 40 (2021) 101778, doi: 10.1016/j.jwpe.2020.101778.
[13] A. Tawfik, Degradation pathways of 1,4-dioxane in biological and advanced oxidation processes, Desal. Water Treat., 178 (2020) 360–386.
[14] S. Giannakis, K.-Y. Andrew Lin, F. Ghanbari, A review of the recent advances on the treatment of industrial wastewaters by sulfate radical-based advanced oxidation processes (SR-AOPs), Chem. Eng. J., 406 (2021) 127083, doi: 10.1016/j.cej.2020.127083.
[15] S. Khelifi, A. Choukchou-Braham, H.M. Sbihi, M. Azam, S.I. Al-Resayes, F. Ayari, Treatment of textile dyeing wastewater using advanced photo-oxidation processes for decolorization and COD reduction, Desal. Water Treat., 217 (2021) 350–357.
[16] M.M. M'Arimi, C.A. Mecha, A.K. Kiprop, R. Ramkat, Recent trends in applications of advanced oxidation processes (AOPs) in bioenergy production: review, Renewable Sustainable Energy Rev., 121 (2020) 109669, doi: 10.1016/j.rser.2019.109669.
[17] L. Qin, R. Ru, J.W. Mao, Q. Meng, Z. Fan, X. Li, G.L. Zhang, Assembly of MOFs/polymer hydrogel derived Fe_3O_4-CuO@ hollow carbon spheres for photochemical oxidation: freezing replacement for structural adjustment, Appl. Catal., B, 269 (2020) 118754, doi: 10.1016/j.apcatb.2020.118754.
[18] J. Kozak, M. Wlodarczyk-Makula, Comparison of the PAHs degradation effectiveness using CaO_2 or H_2O_2 under the photo-Fenton reaction, Desal. Water Treat., 134 (2018) 57–64.
[19] C. Chen, T. Cheng, L. Wang, Y. Tian, Q. Deng, Y. Shi, Application of MoO_3 as an efficient catalyst for wet air oxidation treatment of pharmaceutical wastewater (Experimental and DFT study), Arch. Environ. Prot., 47 (2021) 47–60.
[20] M. Sabaghi, Z. Aghajani, G.R. Najafi, Fabrication of a new heterogeneous tungstate-based on the amino-functionalized metal-organic framework as an efficient catalyst towards sonochemical oxidation of alcohols under green condition, J. Organomet. Chem., 925 (2020) 121483, doi: 10.1016/j.jorganchem.2020.121483.
[21] Q.D. Yao, X.L. Ma, H.X. Wang, Y.R. Wang, G.L. Wang, J. Zhang, W.K. Liu, X.L. Wang, J. Yan, Y.L. Li, W.W. Wang, Investigate on the mechanism of $HfO_2/Si_{0.7}Ge_{0.3}$ interface passivation based on low-temperature ozone oxidation and Si-Cap methods, Nanomaterials, 11 (2021) 955, doi: 10.3390/nano11040955.
[22] M. Mehrdadian, S. Khazalpour, A. Amani, M. Jamshidi, Electrochemical oxidation of 4-ethynylaniline: a green electrochemical protocol for the synthesis of diazine compounds, Electrochim. Acta, 381 (2021) 138242, doi: 10.1016/j.electacta.2021.138242.
[23] H.Y. Shen, P.J. Sun, X. Meng, J.L. Wang, H.Y. Liu, L.J. Xu, Nanoscale Fe^0/Cu^0 bimetallic catalysts for Fenton-like oxidation of the mixture of nuclear-grade cationic and anionic exchange resins, Chemosphere, 269 (2021) 128763, doi: 10.1016/j.chemosphere.2020.128763.
[24] X. Dong, Y.C. Lin, G.L. Ren, Y.Q. Ma, L. Zhao, Catalytic degradation of methylene blue by Fenton-like oxidation of Ce-doped MOF, Colloids Surf., A, 608 (2021) 125578, doi: 10.1016/j.colsurfa.2020.125578.
[25] J. Wu, M. Lin, X.L. Weng, G. Owens, Z.L. Chen, Pre-adsorption and Fenton-like oxidation of mitoxantrone using hybrid green synthesized rGO/Fe nanoparticles, Chem. Eng. J., 408 (2021) 127273, doi: 10.1016/j.cej.2020.127273.
[26] D.L. Huang, C.J. Hu, G.M. Zeng, M. Cheng, P.A. Xu, X.M. Gong, R.Z. Wang, W.J. Xue, Combination of Fenton processes and biotreatment for wastewater treatment and soil remediation, Sci. Total Environ., 574 (2017) 1599–1610.
[27] P.V. Nidheesh, R. Gandhimathi, S.T. Ramesh, Degradation of dyes from aqueous solution by Fenton processes: a review, Environ. Sci. Pollut. Res., 20 (2013) 2099–2132.
[28] L. Zhang, F. Su, N. Wang, S. Liu, M. Yang, Y.-Z. Wang, D.Q. Huo, T.T. Zhao, Biodegradability enhancement of hydrolyzed polyacrylamide wastewater by a combined Fenton-SBR treatment process, Bioresour. Technol., 278 (2019) 99–107.
[29] J.J. Rueda-Márquez, I. Levchuk, M. Manzano, M. Sillanpää, Toxicity reduction of industrial and municipal wastewater by advanced oxidation processes (photo-Fenton, UVC/H_2O_2, electro-Fenton and galvanic Fenton): a review, Catalysts, 10 (2020) 612, doi: 10.3390/catal10060612.
[30] W. Du, R. Huang, X.L. Huang, R. Chen, F.X. Chen, Copper-promoted heterogeneous Fenton-like oxidation of Rhodamine B over Fe_3O_4 magnetic nanocatalysts at mild conditions, Environ. Sci. Pollut. Res., 28 (2021) 19959–19968.
[31] Z.H. Lu, X.F. Cao, H. Wei, W.T. Huo, Q.Q. Wang, K.B. Li, Strong enhancement effect of bisulfite on MIL-68(Fe)-catalyzed Fenton-like reaction for organic pollutants degradation, Appl. Surf. Sci., 542 (2021) 148631, doi: 10.1016/j.apsusc.2020.148631.
[32] L. Peng, X.G. Duan, Y.N. Shang, B.Y. Gao, X. Xu, Engineered carbon supported single iron atom sites and iron clusters from Fe-rich *Enteromorpha* for Fenton-like reactions via nonradical pathways, Appl. Catal., B, 287 (2021) 119963, doi: 10.1016/j.apcatb.2021.119963.
[33] Y.F. Xue, X.G. Gu, S.G. Lu, Z.W. Miao, M.L. Brusseau, M.H. Xu, X.R. Fu, X. Zhang, Z.F. Qiu, Q. Sui, The destruction of benzene by calcium peroxide activated with Fe(II) in water, Chem. Eng. J., 302 (2016) 187–193.
[34] L. Ge, Y. Yue, W. Wang, F.T. Tan, S.H. Zhang, X.Y. Wang, X.L. Qiao, P.K. Wong, Efficient degradation of tetracycline in wide pH range using MgNCN/MgO nanocomposites as novel H_2O_2 activator, Water Res., 198 (2021) 117149, doi: 10.1016/j.watres.2021.117149.
[35] J. Liu, Y. Yue, W. Wang, F. Tan, H. Xia, X. Wang, X. Qiao, P.K. Wong, Facile one-step synthesis of 3D hierarchical flower-like magnesium peroxide for efficient and fast removal of tetracycline from aqueous solution, J. Hazard. Mater., 397 (2020) 122877, doi: 10.1016/j.jhazmat.2020.122877.
[36] J. Zhang, P. Chen, W. Gao, W. Wang, F. Tan, X. Wang, X. Qiao, P.K. Wong, Melamine-cyanurate supramolecule induced graphitic N-rich graphene for singlet oxygen-dominated peroxymonosulfate activation to efficiently degrade organic pollutants, Sep. Purif. Technol., 265 (2021) 118474, doi: 10.1016/j.seppur.2021.118474.
[37] M. Cheng, C. Lai, Y. Liu, G. Zeng, D. Huang, C. Zhang, L. Qin, L. Hu, C. Zhou, W. Xiong, Metal-organic frameworks for highly efficient heterogeneous Fenton-like catalysis, Coord. Chem. Rev., 368 (2018) 80–92.
[38] A.D. Bokare, W. Choi, Review of iron-free Fenton-like systems for activating H_2O_2 in advanced oxidation processes, J. Hazard. Mater., 275 (2014) 121–135.
[39] Y. Feng, D. Wu, L. Ma, Iron oxide catalyzed Fenton-like reaction, Prog. Chem., 25 (2013) 1219–1228.
[40] Y. Zhu, W.H. Fan, W.Y. Feng, Y. Wang, S. Liu, Z.M. Dong, X.M. Li, A critical review on metal complexes removal from water using methods based on Fenton-like reactions: analysis and comparison of methods and mechanisms, J. Hazard. Mater., 414 (2021) 125517, doi: 10.1016/j.jhazmat.2021.125517.
[41] L. Xin, J. Hu, Y. Xiang, C. Li, L. Fu, Q. Li, X. Wei, Carbon-based nanocomposites as Fenton-like catalysts in wastewater treatment applications: a review, Materials, 14 (2021) 2643, doi: 10.3390/ma14102643.
[42] S. Goel, S.I. Zones, E. Iglesia, Encapsulation of metal clusters within MFI via interzeolite transformations and direct

hydrothermal syntheses and catalytic consequences of their confinement, J. Am. Chem. Soc., 136 (2014) 15280–15290.
[43] Z. Wu, S. Goel, M. Choi, E. Iglesia, Hydrothermal synthesis of LTA-encapsulated metal clusters and consequences for catalyst stability, reactivity, and selectivity, J. Catal., 311 (2014) 458–468.
[44] X. Li, E. Iglesia, Pt/[Fe]ZSM-5 modified by Na and Cs cations: an active and selective catalyst for dehydrogenation of n-alkanes to n-alkenes, Chem. Commun. (Camb), (2008) 594–596, doi: 10.1039/B715543C.
[45] S. Goel, Z. Wu, S.I. Zones, E. Iglesia, Synthesis and catalytic properties of metal clusters encapsulated within small-pore (SOD, GIS, ANA) zeolites, J. Am. Chem. Soc., 134 (2012) 17688–17695.
[46] A. Khataee, T.S. Rad, B. Vahid, S. Khorram, Preparation of zeolite nanorods by corona discharge plasma for degradation of phenazopyridine by heterogeneous sono-Fenton-like process, Ultrason. Sonochem., 33 (2016) 37–46.
[47] L. Singh, P. Rekha, S. Chand, Cu-impregnated zeolite Y as highly active and stable heterogeneous Fenton-like catalyst for degradation of Congo red dye, Sep. Purif. Technol., 170 (2016) 321–336.
[48] N.L. Subbulekshmi, E. Subramanian, Nano CuO immobilized fly ash zeolite Fenton-like catalyst for oxidative degradation of *p*-nitrophenol and *p*-nitroaniline, J. Environ. Chem. Eng., 5 (2017) 1360–1371.
[49] Y. Zhang, J. Shang, Y. Song, C. Rong, Y. Wang, W. Huang, K. Yu, Selective Fenton-like oxidation of methylene blue on modified Fe-zeolites prepared via molecular imprinting technique, Water Sci. Technol., 75 (2017) 659–669.
[50] Q. Zhang, Q. Wang, S. Wang, Efficient heterogeneous Fenton-like catalysis of Fe-doped SAPO-44 zeolite synthesized from bauxite and rice husk, Chem. Phys. Lett., 753 (2020) 137598, doi: 10.1016/j.cplett.2020.137598.
[51] B. Shi, C. Zhao, Y. Ji, J. Shi, H. Yang, Promotion effect of PANI on Fe-PANI/Zeolite as an active and recyclable Fenton-like catalyst under near-neutral condition, Appl. Surf. Sci., 508 (2020) 145298, doi: 10.1016/j.apsusc.2020.145298.
[52] Q. Guo, G. Li, D. Liu, Y. Wei, Synthesis of zeolite Y promoted by Fenton's reagent and its application in photo-Fenton-like oxidation of phenol, Solid State Sci., 91 (2019) 89–95.
[53] X. Yang, X. Cheng, A.A. Elzatahry, J. Chen, A. Alghamdi, Y. Deng, Recyclable Fenton-like catalyst based on zeolite Y supported ultrafine, highly-dispersed Fe_2O_3 nanoparticles for removal of organics under mild conditions, Chin. Chem. Lett., 30 (2019) 324–330.
[54] F. Mendez-Arriaga, R. Almanza, Water remediation by UV-Vis/H_2O_2 process, photo-Fenton-like oxidation, and zeolite ZSM5, Desal. Water Treat., 52 (2014) 5822–5832.
[55] C. Chen, T. Cheng, X. Zhang, R. Wu, Q. Wang, Synthesis of an efficient Pb adsorption nano-crystal under strong alkali hydrothermal environment using a Gemini surfactant as directing agent, J. Chem. Soc. Pak., 41 (2019) 1034–1038.
[56] X. Zhang, T. Cheng, C. Chen, L. Wang, Q. Deng, G. Chen, C. Ye, Synthesis of a novel magnetic nano-zeolite and its application as an efficient heavy metal adsorbent, Mater. Res. Express, 7 (2020) 085007.
[57] G. Kresse, J. Furthmüller, Efficient iterative schemes for *ab initio* total-energy calculations using a plane-wave basis set, Phys. Rev. B: Condens. Matter, 54 (1996) 11169–11186.
[58] P. Hohenberg, W. Kohn, Inhomogeneous electron gas, Phys. Rev., 136 (1964) 864–871.
[59] W. Kohn, L.J. Sham, Self-consistent equations including exchange and correlation effects, Phys. Rev., 140 (1965) A1133, doi: 10.1103/PhysRev.140.A1133.
[60] J.P. Perdew, J.A. Chevary, S.H. Vosko, K.A. Jackson, M.R. Pederson, D.J. Singh, C. Fiolhais, Atoms, molecules, solids, and surfaces: applications of the generalized gradient approximation for exchange and correlation, Phys. Rev. B: Condens. Matter, 46 (1992) 6671–6687.
[61] J. Perdew, K. Burke, M. Ernzerhof, Generalized gradient approximation made simple, Phys. Rev. Lett., 77 (1996) 3865–3868.
[62] A. Cabrera-Codony, A. Georgi, R. Gonzalez-Olmos, H. Valdés, M.J. Martín, Zeolites as recyclable adsorbents/catalysts for biogas upgrading: removal of octamethylcyclotetrasiloxane, Chem. Eng. J., 307 (2017) 820–827.
[63] M. Dosa, M. Piumetti, C. Galletti, N. Russo, D. Fino, S. Bensaid, G. Mancini, F.S. Freyria, G. Saracco, A novel Fe-containing clinoptilolite for wastewater remediation: degradation of azo-dyes Acid orange 7 by H_2O_2 and ascorbic acid, Desal. Water Treat., 159 (2019) 121–129.
[64] A. Changduang, T. Limpiyakorn, P. Punyapalakul, P. Thayanukul, Development of reactive iron-coated natural filter media for treating antibiotic residual in swine wastewater: mechanisms, intermediates and toxicity, J. Environ. Manage., 298 (2021) 113435, doi: 10.1016/j.jenvman.2021.113435.
[65] M. Yue, X. Jiang, H. Zhang, S. Zhang, T. Xue, Y. Li, Quasi-solid-phase synthesis of Fe-MFI zeolites by using Fe-containing zeolite seed sol for hydroxylation of benzene with H_2O_2, Microporous Mesoporous Mater., 294 (2020) 109891, doi: 10.1016/j.micromeso.2019.109891.
[66] H. Zhang, Y.F. Fan, Y.H. Huan, M.B. Yue, Dry-gel synthesis of shaped transition-metal-doped M-MFI (M = Ti, Fe, Cr, Ni) zeolites by using metal-occluded zeolite seed sol as a directing agent, Microporous Mesoporous Mater., 231 (2016) 178–185.
[67] M. Mihajlovic, S. Lazarevic, I. Jankovic-Castvan, B. Jokic, D. Janackovic, R. Petrovic, A comparative study of the removal of lead, cadmium and zinc ions from aqueous solutions by natural and Fe(III)-modified zeolite, Chem. Ind. Chem. Eng. Q., 20 (2014) 283–293.
[68] Y. Sun, Q. Fang, J. Dong, X. Cheng, J. Xu, Removal of fluoride from drinking water by natural stilbite zeolite modified with Fe(III), Desalination, 277 (2011) 121–127.
[69] T. Cheng, C. Chen, R. Tang, C.H. Han, Y. Tian, Competitive adsorption of Cu, Ni, Pb, and Cd from aqueous solution onto fly ash-based Linde F(K) zeolite, Iran. J. Chem. Chem. Eng., 37 (2018) 61–72.
[70] C. Chen, Q. Li, L. Shen, J. Zhai, Feasibility of manufacturing geopolymer bricks using circulating fluidized bed combustion bottom ash, Environ. Technol., 33 (2012) 1313–1321.
[71] M. Choi, K. Na, J. Kim, Y. Sakamoto, O. Terasaki, R. Ryoo, Stable single-unit-cell nanosheets of zeolite MFI as active and long-lived catalysts, Nature, 461 (2009) 246–249.
[72] T. Yamashita, P. Hayes, Analysis of XPS spectra of Fe^{2+} and Fe^{3+} ions in oxide materials, Appl. Surf. Sci., 254 (2008) 2441–2449.
[73] J. Liu, Y.M. Yue, L.F. Ge, P. Chen, F.T. Tan, W. Wang, X.Y. Wang, X.L. Qiao, Facile fabrication of magnesium peroxide with different morphologies via the isomorphic transformation of magnesium oxide for Fenton-like degradation of methylene blue, Colloids Surf., A, 607 (2020) 125499, doi: 10.1016/j.colsurfa.2020.125499.
[74] S.J. Zuo, X.M. Jin, X.W. Wang, Y.H. Lu, Q. Zhu, J.W. Wang, W.P. Liu, Y.H. Du, J. Wang, Sandwich structure stabilized atomic Fe catalyst for highly efficient Fenton-like reaction at all pH values, Appl. Catal., B, 282 (2021) 119551, doi: 10.1016/j.apcatb.2020.119551.
[75] R. Gonzalez-Olmos, M.J. Martin, A. Georgi, F.-D. Kopinke, I. Oller, S. Malato, Fe-zeolites as heterogeneous catalysts in solar Fenton-like reactions at neutral pH, Appl. Catal., B, 125 (2012) 51–58.
[76] Y. Gao, S. Li, Y. Li, L. Yao, H. Zhang, Accelerated photocatalytic degradation of organic pollutant over metal-organic framework MIL-53(Fe) under visible LED light mediated by persulfate, Appl. Catal., B, 202 (2017) 165–174.
[77] T. Guo, L. Jiang, K. Wang, Y. Li, H. Huang, X. Wu, G. Zhang, Efficient persulfate activation by hematite nanocrystals for degradation of organic pollutants under visible light irradiation: facet-dependent catalytic performance and degradation mechanism, Appl. Catal., B, 286 (2021) 119883, doi: 10.1016/j.apcatb.2021.119883.
[78] M.L. Rache, A.R. García, H.R. Zea, A.M.T. Silva, L.M. Madeira, J.H. Ramírez, Azo-dye orange II degradation by the heterogeneous Fenton-like process using a zeolite Y-Fe catalyst—kinetics with a model based on the Fermi's equation, Appl. Catal., B, 146 (2014) 192–200.
[79] A. Cihanoğlu, G. Gündüz, M. Dükkancı, Degradation of acetic acid by heterogeneous Fenton-like oxidation over

iron-containing ZSM-5 zeolites, Appl. Catal., B, 165 (2015) 687–699.
[80] M. Dukkanci, G. Gunduz, S. Yilmaz, R.V. Prihod'ko, Heterogeneous Fenton-like degradation of Rhodamine 6G in water using CuFeZSM-5 zeolite catalyst prepared by hydrothermal synthesis, J. Hazard. Mater., 181 (2010) 343–350.
[81] K. Rusevova, R. Köferstein, M. Rosell, H.H. Richnow, F.-D. Kopinke, A. Georgi, $LaFeO_3$ and $BiFeO_3$ perovskites as nanocatalysts for contaminant degradation in heterogeneous Fenton-like reactions, Chem. Eng. J., 239 (2014) 322–331.
[82] A.C. Affam, Effect of hydraulic retention time on nutrients and organics removal by FeGAC/H_2O_2-SBR treatment of pesticide wastewater, Desal. Water Treat., 195 (2020) 297–304.
[83] A. Sheikhmohammadi, E. Asgari, J. Yeganeh, Application of Fe_3O_4@activated carbon magnetic nanoparticles for the adsorption of metronidazole from wastewater: optimization, kinetics, thermodynamics and equilibrium studies, Desal. Water Treat., 222 (2021) 354–365.
[84] Y.J. Zhang, S.H. Hu, X.H. Mi, R. Zhang, R. Sun, Y.G. Wu, Nitrobenzene removal by novel pillared kaolinite-catalyzed Fenton-like reaction, Desal. Water Treat., 218 (2021) 210–219.
[85] X. Wei, X. Xie, Y. Wang, S. Yang, Shape-dependent Fenton-like catalytic activity of Fe_3O_4 nanoparticles, J. Environ. Eng., 146 (2020) 04020005, doi: 10.1061/(ASCE)EE.1943-7870.0001648.
[86] G.A. Ashraf, R.T. Rasool, M. Hassan, L. Zhang, Enhanced photo Fenton-like activity by effective and stable Al–Sm M-hexaferrite heterogenous catalyst magnetically detachable for methylene blue degradation, J. Alloys Compd., 821 (2020) 153410, doi: 10.1016/j.jallcom.2019.153410.
[87] X. Wang, Z. Nan, Highly efficient Fenton-like catalyst Fe-g-C_3N_4 porous nanosheets formation and catalytic mechanism, Sep. Purif. Technol., 233 (2020) 116023, doi: 10.1016/j.seppur.2019.116023.
[88] F.L. Rivera, F.J. Recio, F.J. Palomares, J. Sánchez-Marcos, N. Menéndez, E. Mazarío, P. Herrasti, Fenton-like degradation enhancement of methylene blue dye with magnetic heating induction, J. Electroanal. Chem., 879 (2020) 114773, doi: 10.1016/j.jelechem.2020.114773.
[89] J.-H. Chu, J.-K. Kang, S.-J. Park, C.-G. Lee, Application of magnetic biochar derived from food waste in heterogeneous sono-Fenton-like process for removal of organic dyes from aqueous solution, J. Water Process Eng., 37 (2020) 101455, doi: 10.1016/j.jwpe.2020.101455.
[90] H. Xiang, G. Ren, Y. Zhong, D. Xu, Z. Zhang, X. Wang, X. Yang, Fe_3O_4@C nanoparticles synthesized by in situ solid-phase method for removal of Methylene blue, Nanomaterials (Basel), 11 (2021) 330, doi: 10.3390/nano11020330.
[91] A. Kirchon, P. Zhang, J. Li, E.A. Joseph, W. Chen, H.C. Zhou, Effect of isomorphic metal substitution on the Fenton and photo-Fenton degradation of methylene blue using Fe-based metal–organic frameworks, ACS Appl. Mater. Interfaces, 12 (2020) 9292–9299.
[92] H.A. Bicalho, J.L. Lopez, I. Binatti, P.F.R. Batista, J.D. Ardisson, R.R. Resende, E. Lorençon, Facile synthesis of highly dispersed Fe(II)-doped g-C_3N_4 and its application in Fenton-like catalysis, Mol. Catal., 435 (2017) 156–165.
[93] A.M. Atta, Y.M. Moustafa, H.A. Al-Lohedan, A.O. Ezzat, A.I. Hashem, Methylene blue catalytic degradation using silver and magnetite nanoparticles functionalized with a poly(ionic liquid) based on quaternized dialkylethanolamine with 2-acrylamido-2-methylpropane sulfonate-co-vinylpyrrolidone, Omega, 5 (2020) 2829–2842.
[94] D. Li, T. Yang, Y. Li, Z. Liu, W. Jiao, Facile and green synthesis of highly dispersed tar-based heterogeneous Fenton catalytic nanoparticles for the degradation of methylene blue, J. Cleaner Prod., 246 (2020) 119033, doi: 10.1016/j.jclepro.2019.119033.
[95] Y. Wu, L. Fan, S. Hu, S. Wang, H. Yao, K. Wang, Role of dissolved iron ions in nanoparticulate zero-valent iron/H_2O_2 Fenton-like system, Int. J. Environ. Sci. Technol., 16 (2019) 4551–4562.
[96] J. Zhang, W. Gao, Y. Yue, W. Wang, F. Tan, X. Wang, X. Qiao, P.K. Wong, Two-step assembly induced Fe^0-anchored graphitic N-rich graphene with biactive centers for enhanced heterogeneous peroxymonosulfate activation, J. Mater. Chem. A, 9 (2021) 17366–17379.
[97] M. Qin, B. Lu, S. Feng, Z. Zhen, R. Chen, H. Liu, Role of exposed facets and surface OH groups in the Fenton-like reactivity of lepidocrocite catalyst, Chemosphere, 230 (2019) 286–293.
[98] Y. Chen, Z. Yang, Y.B. Liu, Y. Liu, Fenton-like degradation of sulfamerazine at nearly neutral pH using Fe-Cu-CNTs and Al^0-CNTs for in-situ generation of H_2O_2/•OH/$O_2^{\bullet-}$, Chem. Eng. J., 396 (2020) 125329, doi: 10.1016/j.cej.2020.125329.
[99] Z. Dong, C. Jiang, Q. Guo, J. Li, X. Wang, Z. Wang, J. Jiang, A novel diagnostic method for distinguishing between Fe(IV) and •OH by using atrazine as a probe: clarifying the nature of reactive intermediates formed by nitrilotriacetic acid assisted Fenton-like reaction, J. Hazard. Mater., 417 (2021) 126030, doi: 10.1016/j.jhazmat.2021.126030.
[100] W.H. Feng, J. Yuan, L.L. Zhang, W.T. Hu, Z.H. Wu, X.L. Wang, X.Y. Huang, P. Liu, S.Y. Zhang, Atomically thin ZnS nanosheets: facile synthesis and superior piezocatalytic H_2 production from pure H_2O, Appl. Catal., B, 277 (2020) 119250, doi: 10.1016/j.apcatb.2020.119250.
[101] L. Duan, G. Li, S. Zhang, H. Wang, Y. Zhao, Y. Zhang, Sulfur-doped photocatalysts with iron-nitrogen coordination bonds by modifying graphitic carbon nitride obtained from ammonium thiocyanate pyrolysis with ferrous sulfate heptahydrate in ethanol, Opt. Mater., 118 (2021) 111222, doi: 10.1016/j.optmat.2021.111222.
[102] Z. Wang, L. Jiang, K. Wang, Y. Li, G. Zhang, Novel AgI/$BiSbO_4$ heterojunction for efficient photocatalytic degradation of organic pollutants under visible light: interfacial electron transfer pathway, DFT calculation and degradation mechanism study, J. Hazard. Mater., 410 (2021) 124948, doi: 10.1016/j.jhazmat.2020.124948.
[103] H. Huang, T. Guo, K. Wang, Y. Li, G. Zhang, Efficient activation of persulfate by a magnetic recyclable rape straw biochar catalyst for the degradation of tetracycline hydrochloride in water, Sci. Total Environ., 758 (2021) 143957, doi: 10.1016/j.scitotenv.2020.143957.

Supplementary information

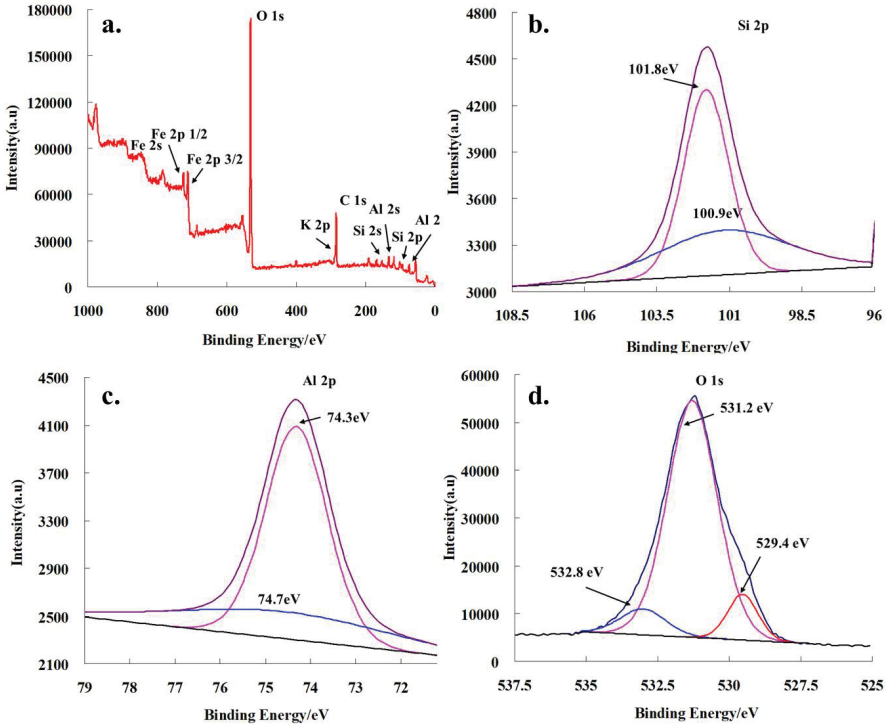

Fig. S1. Full XPS spectrum scanning analysis of zeolite@Fe after 4th reaction (a) and the high-resolution XPS spectra of Si2p (b), Al2p (c), and O1s (d).

S1. Methods of reducing the impact of Fe leaching on water environment

After each run, 0.005 g original zeolite was added into system to adsorb leaching Fe element. Then, the mixture solid was filtered out from the solution by 0.45 μm filter membrane, and the filer solids were washed by deionized water for several times. Then, the recycling sample (zeolite@ Fe/zeolite) was dried to constant weight at a temperature of 85°C in the blast drying oven for the next cycle. After testing, the concentration of Fe in the solution could be reduced to less than 0.3 mg L^{-1}, which would have little impact on the regional water environment. Meanwhile, Fig. S2 shows the MB degradation results of recycling zeolite@Fe/zeolite catalyst. From Fig. S2, it could be seen that the degradation result of MB was more stable when original zeolite was added in the process of recycling.

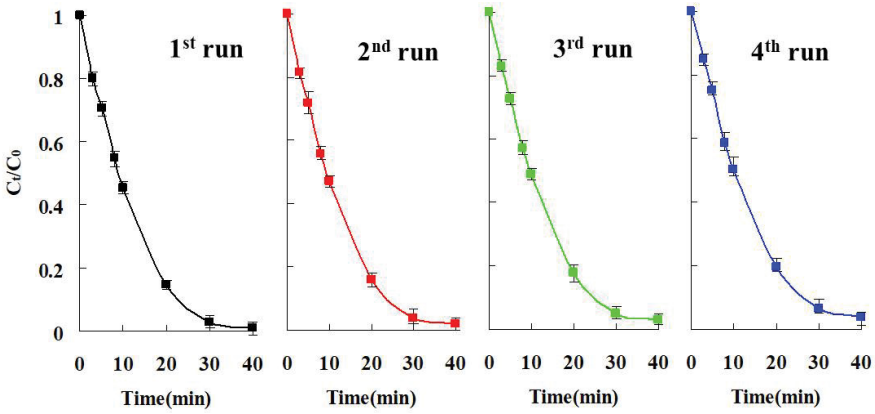

Fig. S2. MB degradation results of recycling zeolite@Fe/zeolite catalyst.